Peroxiredoxin promotes longevity and H_2O_2-resistance in yeast through redox-modulation of protein kinase A

Friederike Roger[1], Cecilia Picazo[1,2], Chikako Asami[1], Wolfgang Reiter[3], Sarah Hanzén[1], Chunxia Gao[1], Gilles Lagniel[4], Niek Welkenhuysen[5], Jean Labarre[4], Thomas Nyström[6], Morten Grøtli[1], Markus Hartl[3] and Mikael Molin*[1,2]

[1]Department of Chemistry and Molecular Biology, University of Gothenburg, SWEDEN

[2]Department of Biology and Biological Engineering, Chalmers University of Technology, Gothenburg, SWEDEN

[3]Mass Spectrometry Facility, Department of Biochemistry, Max F. Perutz Laboratories, University of Vienna, Vienna BioCenter, Vienna, AUSTRIA

[4]Oxidative Stress and Cancer Laboratory, Integrative Biology and Molecular Genetics Unit (SBIGEM), CEA Saclay, FRANCE

[5]Department of Mathematical Sciences, Chalmers University of Technology and University of Gothenburg, SWEDEN

[6]Department of Microbiology and Immunology, Institute for Biomedicine, Sahlgrenska Academy, University of Gothenburg

*Correspondence: mikael.molin@chalmers.se

Keywords

Aging, peroxiredoxin, H_2O_2 signaling, protein kinase A, glutathionylation, hormesis

Abstract

Peroxiredoxins are major peroxide scavenging enzymes and mediators of the beneficial effects of caloric restriction on aging. By which mechanism peroxiredoxins stimulate H_2O_2 resistance and slow down aging is, however, incompletely understood. Here we show that the yeast peroxiredoxin Tsa1 boosts H_2O_2 tolerance and delays aging not by its action of scavenging H_2O_2, but by repressing the nutrient signaling protein kinase A (PKA). Tsa1 represses PKA activity through redox modification of the catalytic subunits and a significant proportion of catalytic subunits are glutathionylated on two cysteine residues. Redox modification of the conserved Cys243 in the catalytic subunits inhibits the phosphorylation of a conserved Thr241 in the kinase activation loop and enzyme activity and preventing Thr241 phosphorylation can overcome the H_2O_2 sensitivity of Tsa1-deficient cells. Results support a model of aging where nutrient signaling pathways constitute hubs integrating information from multiple aging-related conduits including a peroxiredoxin-dependent responding to H_2O_2.

Introduction

Caloric restriction (CR) is an intervention that slows down aging and reduces the incidence of age-related disease in most organisms, from the unicellular baker's yeast (Lin, Defossez, & Guarente, 2000) to rhesus monkeys (Mattison et al., 2017).

CR-induced reduced nutrient signaling via insulin/insulin-like growth factor (IGF-1), the target-of-rapamycin and/or protein kinase A pathways is intimately linked to lifespan extension (L. Fontana, Partridge, L., and Longo, V.D., 2010; Kenyon, 2010; Molin & Demir, 2014; Nystrom, Yang, & Molin, 2012). Of other things, reduced nutrient signaling mitigates age-related oxidative damage by increasing oxidative stress resistance in organisms from yeast to humans (Fontan-Lozano, Lopez-Lluch, Delgado-Garcia, Navas, & Carrion, 2008; Heilbronn et al., 2006; Molin et al., 2011; Schulz et al., 2007; Sohal & Forster, 2014), and this effect appears as a common denominator of the nutrient signaling pathways that dictate the anti-aging effects of CR and its health benefits (Alic & Partridge, 2011; L. Fontana, Partridge, & Longo, 2010; Longo, Shadel, Kaeberlein, & Kennedy, 2012). Still very few specific targets of nutrient signaling explaining the beneficial effects of CR have been identified (L. Fontana et al., 2010).

In this respect it is interesting that the peroxiredoxins, which constitute a major family of peroxide-negotiating anti-oxidant enzymes, are required for lifespan promotion by CR and CR-mimetics (De Haes et al., 2014; Molin et al., 2011; Olahova & Veal, 2015). For instance, in worms, the CR-mimetic drug metformin extends lifespan in a manner dependent on the activity of Prdx-2 (De Haes et al., 2014), and in flies, neuronal peroxiredoxin overexpression extends lifespan in the absence of caloric restriction (Lee et al., 2009). We previously showed in yeast that CR increases both H_2O_2 tolerance and lifespan by stimulating the activity of the major 2-Cys peroxiredoxin, Tsa1 (Molin et al., 2011). In addition, mild overexpression of Tsa1 potently extended lifespan (40%) (Hanzen et al., 2016), which led us to ask by which mechanism peroxiredoxins reduce the rate of aging? As major cellular peroxide scavenging enzymes, peroxiredoxins are required for the maintenance of genome stability (Molin & Demir, 2014; Nystrom et al., 2012) and PrxI-deficient mice prematurely accumulate age-related tumors (Neumann et al., 2003). However, mild Tsa1 overexpression, although increasing lifespan, did not alter the rate at which mutations accumulate during aging (Hanzen et al., 2016). Furthermore, CR reduces the increased mutation rate in Tsa1-deficient cells by 50% (Hanzen et al., 2016) without extending their life-span (Molin et al., 2011). We instead proposed that Tsa1 acquires the ability to counteracts age-related protein damage by guiding Hsp70/104 molecular chaperones to proteins aggregating upon increased age and H_2O_2 (Hanzen et al., 2016).

Prx are obligate dimers carrying two cysteines, one of which reduces H_2O_2, thereby forming a sulfenic acid (C48-SOH in yeast Tsa1), which condenses with the other cysteine of the second Prx molecule (Cys171) into an inter-subunit disulfide, reduced by thioredoxin. Once the Cys48-SOH is formed it can react with another molecule of H_2O_2 to form a sulfinic acid (Cys48-SOOH), instead of condensing into a disulfide. Sulfinylation inactivates the enzyme catalytic cycle, switching it into a molecular chaperone by multimerisation (Hanzen et al., 2016; Jang et al., 2004; Noichri et al., 2015). In addition to their scavenging and chaperone functions, Prxs have also been shown to signal hydrogen peroxide by transfer of the oxidant signal to target proteins (Leichert & Dick, 2015; Stocker, Van Laer, Mijuskovic, & Dick, 2017). We recently showed that, in response to H_2O_2, Tsa1 and thioredoxin were required to inhibit PKA-mediated repression of the transcription factor Msn2 leading to its activation (Bodvard et al., 2017), and in worms, increased Prdx-2 function upon metformin treatment was connected to increased PMK-1/p38 mitogen-activated protein kinase (MAPK) activity (De Haes et al., 2014).

Here we explored whether the H_2O_2 signaling function of Tsa1 had any relevance in its role in H_2O_2 resistance and in slowing down aging. We show that the hydrogen peroxide sensitivity and premature aging in cells lacking Tsa1 is due to aberrant nutrient signaling through protein kinase A (PKA), and not to defective H_2O_2 scavenging per se. Tsa1 interacts with PKA at the level of its catalytic subunits. We identified a conserved cysteine in the most highly expressed PKA catalytic subunit that is specifically required for Tsa1-mediated H_2O_2 resistance. Tsa1-dependent redox-modification of this Cys residue reduced enzyme activity and increased H_2O_2 resistance in part through dephosphorylating a conserved threonine (Thr241) in the kinase activation loop. These results indicate that peroxiredoxins slow down the rate of aging through a unique role in kinase signaling and suggest a novel mode of regulation of the conserved nutrient-sensing cascade PKA bypassing conventional signaling via the second messenger cAMP and impinging on H_2O_2 resistance and aging.

Results

Tsa1 slows down aging in a manner dependent on both catalytic cysteines but independent on H_2O_2 scavenging

To clarify the mechanism by which Tsa1 promotes longevity, we analyzed the lifespans of *tsa1C48S* (Cys48Ser) and *tsa1C171S* (Cys171Ser) mutants (Fig. 1A). In agreement with a crucial role of the catalytic cysteines in lifespan control *tsa1C48S* and *tsa1C171S* cells suffered a lifespan as short as cells lacking Tsa1 altogether (Fig. 1A). In addition, cells expressing a truncated form of Tsa1 lacking the C-terminal YF motif (*tsa1ΔYF*), which is not sensitive to sulfinylation (Hanzen et al., 2016), had a near wild-type lifespan, supporting the idea that both Tsa1 catalytic cysteines and only to a minor extent Tsa1C48 sulfinylation are important for peroxiredoxin-mediated control of the rate of aging. We next inquired whether the H_2O_2-sensitivity and short lifespan of cells lacking Tsa1 was caused by defective H_2O_2-scavenging. In a first assay, we exposed cells to H_2O_2 and monitored its decay in the extracellular milieu. Like cells expressing an extra copy of *TSA1* (Hanzen et al., 2016), Tsa1-deficient cells reduced exogenous H_2O_2 as efficiently as did wild-type cells (Fig. 1B). To measure H_2O_2 levels

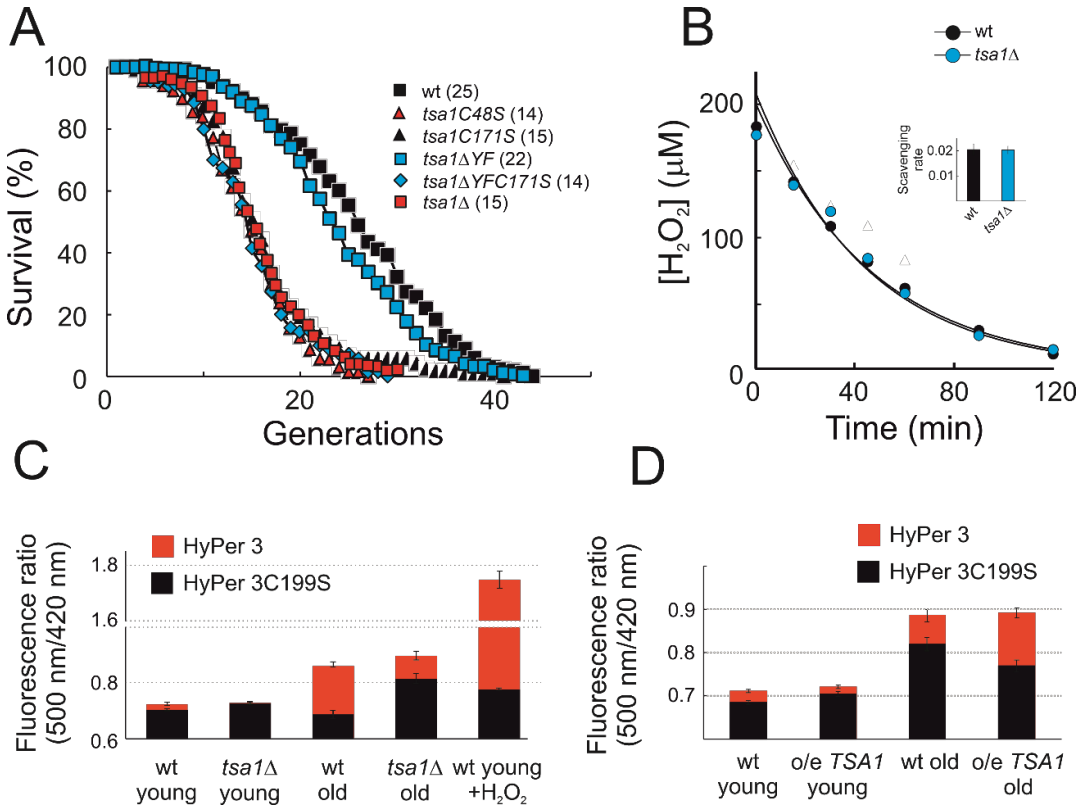

Figure 1. The peroxiredoxin Tsa1 slows down aging in a manner dependent on catalytic cycling but independent on H_2O_2-scavenging. **A)** Life spans of wild-type or the indicated genomic *TSA1* mutant strains (n=120-293). **B)** H_2O_2 scavenging measured as the removal of medium H_2O_2. A representative curve for cultures to which 200 μM was added is shown. Inset shows average scavenging rates for cultures to which 400 μM was added (n=3). Error bars indicate SD. **C)** Average HyPer3 (red) or HyPer3 C199S (black) fluorescence ratio (500 nm/420 nm) in young or old wild-type or *tsa1Δ* cells in the absence of H_2O_2 or following the addition of 400 μM H_2O_2 for 10 min. Cells of about 10-12 generations of replicative age (old) or young control cells (young) were isolated by the biotin-streptavidin method. Error bars indicate standard error of the mean (n=170-619). **D)** Average HyPer3 (red) or HyPer3 C199S (black) fluorescence ratio (500 nm/420 nm) in young or old wild-type (YMM130) and o/e *TSA1* cells isolated as in **C)**. Error bars indicate standard error of the mean (n=381-579).

in cells lacking Tsa1 specifically in the context of aging we expressed the genetically encoded H_2O_2 sensor HyPer3 (Bilan et al., 2013) in aged cells. In wild-type cells of about 10 generations of age we observed a modest but significant increase in the H_2O_2 specific HyPer signal compared to young control cells. Tsa1-deficient cells suffered a similar or lower increase in the H_2O_2-specific fluorescence ratio, relative to the wild-type. In cells expressing an extra copy of the *TSA1* gene, which exhibit an about 40% extended lifespan compared to control cells (Hanzen et al., 2016), the H_2O_2-specific HyPer3 signal increased to a similar or increased extent in aged cells (Fig. 1D). We conclude that Tsa1 is required in aging control as a fully catalytically-active enzyme, although this requirement is not linked to the cellular H_2O_2 scavenging capacity.

Increased H_2O_2 sensitivity and premature aging in cells lacking Tsa1 are both counteracted by Ras deficiency

PKA antagonizes both longevity (Lin et al., 2000) and resistance to H_2O_2 (Molin et al., 2011). Furthermore, Tsa1 is required for the PKA-dependent phosphorylation of the transcription factor Msn2 in response to H_2O_2 (Bodvard et al., 2017). We thus evaluated whether PKA activity contributes to the short lifespan and H_2O_2-sensitivity of Tsa1-deficient cells. We combined the deletion of *RAS2*, which largely abrogates glucose stimulation of PKA and keeps PKA-activity at a low level still compatible with growth [Fig. 2A, (Santangelo, 2006)], and of *TSA1*. Interestingly, Ras2 deficiency completely counteracted the reduced lifespan (Fig. 2B) and H_2O_2-sensitivity (Fig. 2C-D, Fig. S1A) of cells lacking Tsa1, suggesting that these phenotypes of cells lacking Tsa1 were caused by aberrantly increased PKA activity. Ras2 deficiency was also able to partly overcome the H_2O_2 sensitivity of cells lacking both cytosolic thioredoxins (Fig. S1B), which recycle oxidized Prxs during catalytic cycling. As Ras2 might control aging by a PKA-independent pathway

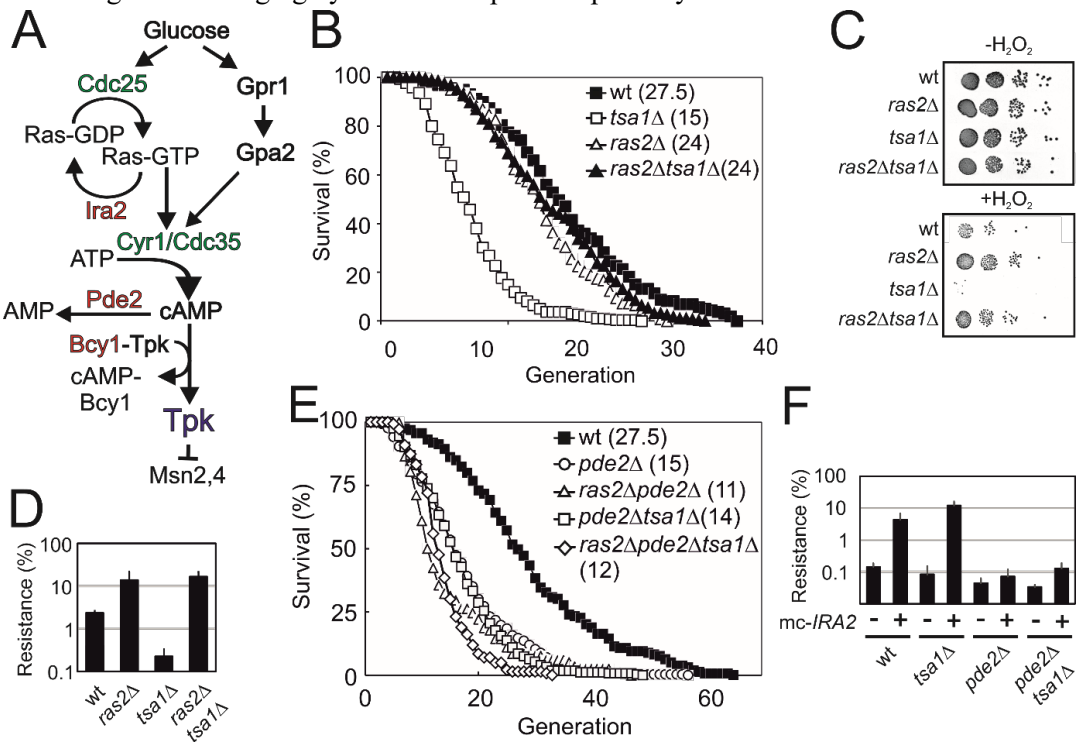

Figure 2. The accelerated aging and H_2O_2 sensitivity of cells lacking Tsa1 can be counteracted by reducing protein kinase A activity. **A.** Overview of the Ras-cAMP-PKA signaling pathway. In green stimulatory components and in red inhibitory. **B, F)** Lifespan of cells lacking Tsa1, Ras2, Pde2 or combinations thereof (n=120-293). **C-D)** H_2O_2 resistance of cells lacking Tsa1, Ras2 or both at the indicated culture density. **E-F)** Quantification of H_2O_2 -resistance (n=3). **F)** H_2O_2 resistance of the indicated mutant cells overexpressing *IRA2* (mc-*IRA2* **+**) or the vector control (**-**), (n=3).

(Sun, Kale, Childress, Pinswasdi, & Jazwinski, 1994), we tested whether the suppression of the short lifespan and H_2O_2-sensitivity in Tsa1-deficient cells conferred by Ras2-deficiency was linked to reduced PKA activity. To this end we deleted the high affinity cAMP-phosphodiesterase *PDE2* in cells lacking Ras2 and Tsa1 to independently increase PKA activity. *PDE2* deletion restored both the H_2O_2-sensitivity (Fig. S1C) and the accelerated aging of Tsa1-deficient cells (Fig. 2E). Furthermore, Pde2 deficiency and Tsa1-deficiency appeared to impinge on the same pathway of aging-control since cells lacking either of these two proteins were as short-lived (Fig. 2E) and H_2O_2-sensitive (Fig. S1C) as cells lacking both. Similar to *RAS2* deletion, overproduction of the Ras-GTPase activating protein (GAP) Ira2, which reduces the levels of active Ras (Ras-GTP, Fig. 2A) was also able to overcome H_2O_2 sensitivity of cells lacking Tsa1 (Fig. 2F) in a manner dependent on decreased PKA activity, since *pde2Δtsa1Δ* cells overproducing Ira2 were sensitive to H_2O_2 (Fig. 2F). We conclude that H_2O_2-sensitivity and the short lifespan of cells lacking Tsa1 is linked to aberrantly increased PKA activity.

The slow growth of Ras-deficient cells is caused by inhibition of PKA by Tsa1

Cells lacking Ras2 grew significantly slower than the wild-type (Fig. 3A, Fig. S1C), consistent with a substantial reduction in PKA activity. In contrast, cells lacking both Ras2 and Tsa1 grew at a rate

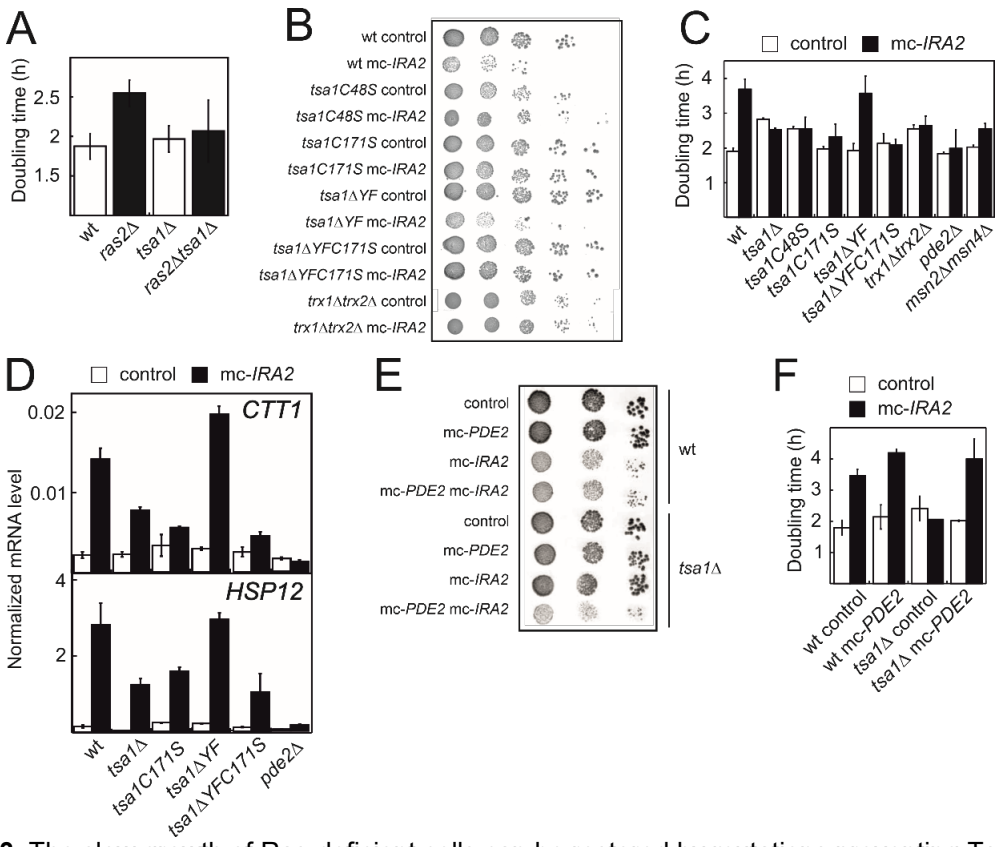

Figure 3. The slow growth of Ras-deficient cells can be restored by mutations preventing Tsa1 catalytic cycling and its inhibitory effect on PKA signaling. **A)** Growth rates of cells lacking Ras2, Tsa1 or both (n=3, error bars indicate SD). **B-C)** Growth rates of cells overexpressing *IRA2* in the indicated mutants of the Tsa1 catalytic cycle or the PKA signaling pathway on solid (**B**) or in liquid medium (**C**, n=3-7). **D)** Expression of the PKA repressed *CTT1* or *HSP12* genes in the indicated mutants in the Tsa1 catalytic cycle overexpressing *IRA2* (mc-*IRA2*) or not (instead expressing the vector, control, n=3±SD) sampled during mid-exponential growth. **E-F)** Growth of Tsa1-proficient or deficient (*tsa1Δ*) cells overexpressing *IRA2* (mc-*IRA2*) or *PDE2* (mc-*PDE2*), both or the corresponding vector control plasmids (control) on solid medium (**E**) or in liquid medium (**F**, n=3±SD).

indistinguishable from that of Tsa1-deficient cells (Fig. 3A), which suggests both that Tsa1 inhibits PKA activity, and that this occurs in a manner independent of Ras2. To further substantiate this result, we checked the effect of Tsa1 deficiency in cells in which Ras and PKA were inactivated as a result of Ira2 overexpression. The latter condition slowed down growth to approximately half the rate of control cells, but strikingly deleting *TSA1* restored growth to wild type levels (Fig. 3B-C, Fig. S2A-B). As an indication that this rescue involves increased PKA activity, expression of the PKA-repressed Msn2/4 target genes decreased in such cells (Fig. 3D, Fig. S2C). Furthermore, overproducing both Pde2 and Ira2 in cells lacking Tsa1 slowed down growth to the rates of wild-type cells overproducing Ira2, also indicating that the rescue of the slow growth of Ras2-deficient cells by deletion of Tsa1 is due to increased PKA activity (Fig. 3E-F). The above results thus indicate that Tsa1 inhibits PKA. We next enquired whether this effect required Tsa1 catalytic Cys residues by overproducing Ira2 in Tsa1-catalytic cysteines C48 and C171 mutants or in cells expressing Tsa1YF (*tsa1ΔYF*). Strikingly, as its null deletion, *tsa1C171S* substitution suppressed the slow growth of Ira2 overproducing cells (Fig. 3B-C) and reduced the expression of the PKA-repressed genes *CTT1* and *HSP12* (Fig. 3D), in contrast to *tsa1ΔYF*, that had no effect on any of these parameters (Fig. 3B-D). Tsa1-mediated H_2O_2-signaling to PKA requires thioredoxin (Bodvard et al., 2017) and in analogy with this, slow growth (Fig. 3B-C) and the increased expression of Msn2/4 targets (Fig. S2C) upon Ras-deficiency were absolutely dependent on the presence of cytosolic thioredoxins (Trx1 and Trx2). Taken together, the data suggest that in Ras-deficient cells catalytically active Tsa1 restrain PKA-dependent activity through a mechanism involving the thioredoxins.

A single extra copy of *TSA1* slows down aging by mildly reducing PKA activity

We previously observed that a single extra-copy of the *TSA1* gene substantially extends lifespan in the absence of caloric restriction (Hanzen et al., 2016). We thus asked whether this effect was due to Tsa1-dependent PKA inhibition. Deleting *PDE2* indeed prevented the increased lifespan seen in the wild type upon mild *TSA1* overexpression (Fig. 4A, 6.7 ± 1%, longer lifespan in *pde2Δ* o/e *TSA1* versus *pde2Δ* control cells, n=3). As further evidence that cells mildly overexpressing Tsa1 exhibit decreased PKA activity, both the accumulation of the reserve carbohydrate glycogen (Fig. 4B) and the expression of the PKA-repressed Msn2/4 target Hsp12 (Fig. 4C) increased. In addition, such cells were resistant to H_2O_2 (Fig. 4D). These effects were lost in cells also lacking Pde2, thus indicating that they are indeed caused by a reduction in PKA activity (Fig. 4C-D).

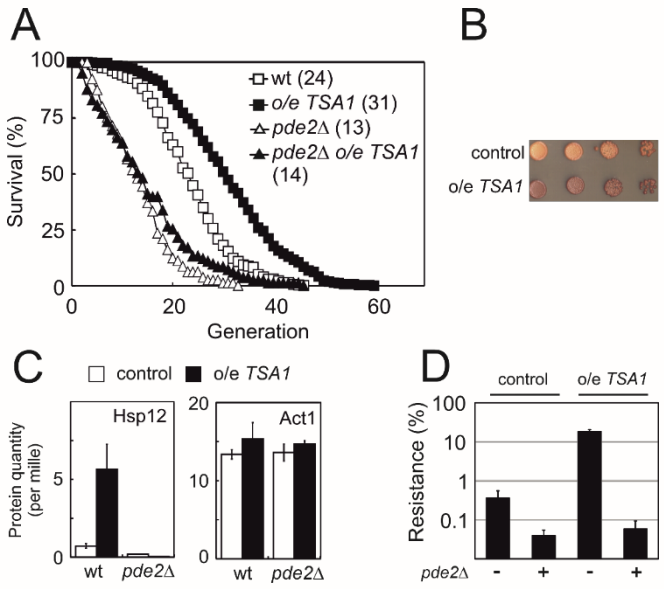

Figure 4. An extra copy of the *TSA1* gene represses PKA signaling, increases H_2O_2 resistance and extends lifespan in a manner dependent on reduced PKA signaling. **A)** Lifespans of cells expressing an extra copy of the *TSA1* gene or not (vector control) in combination with the deletion of *PDE2* to induce high PKA signaling (*pde2Δ*, n=92-439). **B)** Accumulation of glycogen in vector control cells or cells expressing an extra copy of the *TSA1* gene as assayed by iodine vapor. **C)** Expression of Hsp12 in the indicated mutant strains (n=3). **D)** H_2O_2 resistance in the indicated mutant strains (n=3).

Tsa1 affects PKA activity independent of active Ras and cAMP

To establish at which level in the pathway Tsa1 affects PKA activity, we measured the levels of the pathway signaling intermediates in cells overproducing Ira2 in the presence and absence of Tsa1. As expected, overexpression of *IRA2* dramatically reduced the levels of active Ras (Ras-GTP) and this reduction was largely maintained in *pde2Δ* cells (Fig. 5A), in which PKA signaling is increased

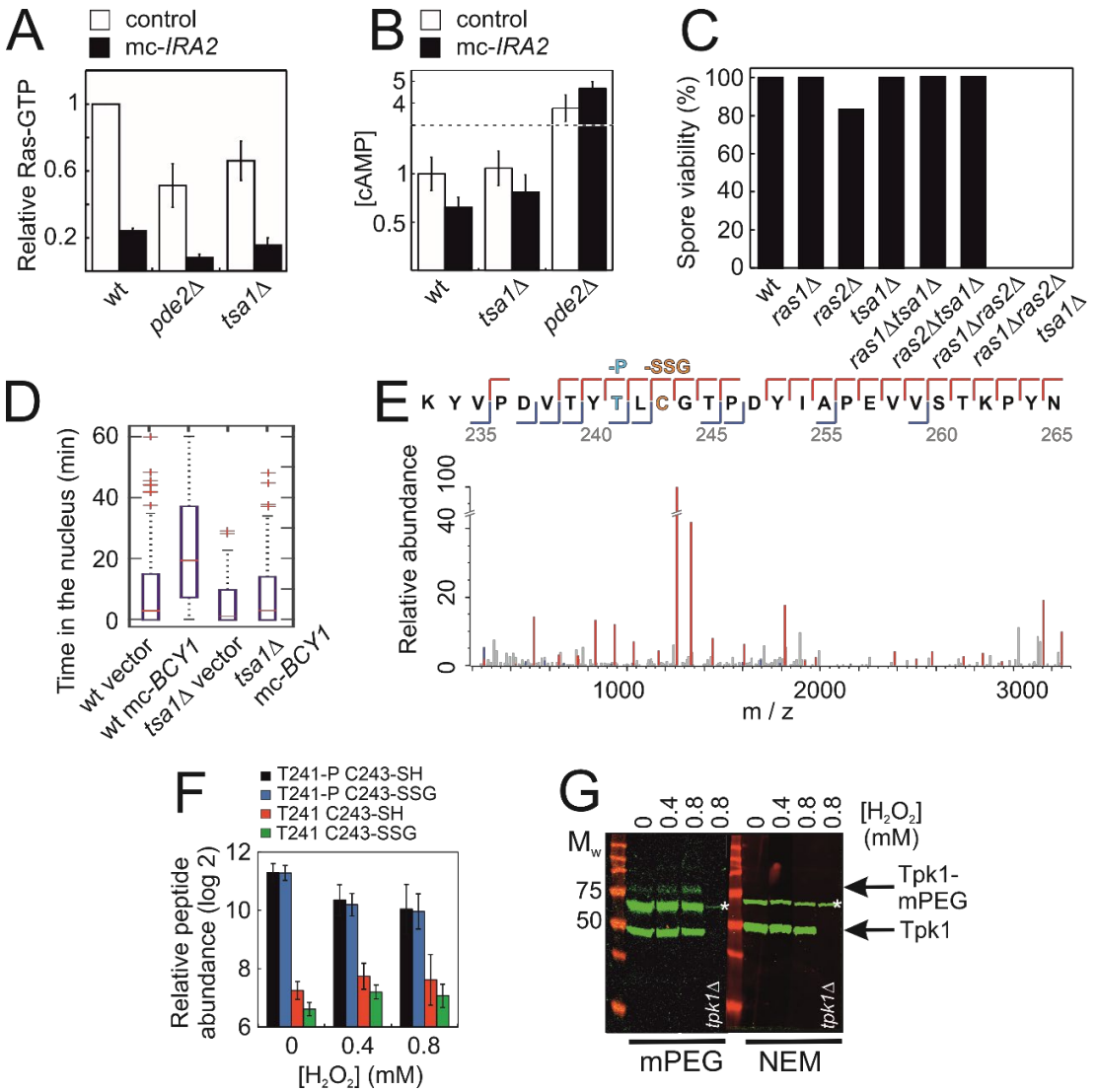

Figure 5. Tsa1 modulates PKA activity at the level of the catalytic subunit Tpk1 and Tpk1 is glutathionylated at a conserved cysteine. **A-B)** Ras-GTP (**A**) or cAMP (**B**) levels in the wild-type or the indicated mutant strains overexpressing *IRA2* (mc-*IRA2*) or not (expressing the vector control, control). **C)** Spore viability of cells deficient in Ras1, Ras2, Tsa1 or combinations thereof. Viability was estimated in 32 tetrads where genotypes could be assigned to all spores (128 in total, 8-23 spores per genotype). **D)** Total time of nuclear Msn2 localization in the indicated mutant strains for 60 min following the addition of 0.3 mM H_2O_2. **E**) MS-MS spectrum showing the matching b-ion (blue) and y-ion (red) series following fragmentation of the Thr241 phosphorylated and C243 glutathionylated peptide encompassing amino acid residues Y239-K261 in Tpk1. T-P = phospho-threonine, C-SSG = glutathionylated cysteine. **F)** PRM-based quantification of the indicated Thr241 and Cys243 containing Y239-K261 peptides in Tpk1, in the absence or presence of the indicated amount of H_2O_2, respectively (n=3). Error bars indicate SD. **G)** mPEG assay of the oxidation of Tpk1 following the addition of the indicated amount of H_2O_2 for 10 min. Cells were treated with H_2O_2, lysed by TCA and reduced cysteines alkylated by NEM. Following reduction by DTT, oxidized cysteines were alkylated by mPEG in half of the extract (mPEG) and to the other half NEM was added as a control (NEM).

downstream of Ras. Similarly, Tsa1-deficient cells overproducing Ira2 exhibited very low Ras-GTP levels (Fig. 5A). In addition, cAMP levels were barely affected in Tsa1-deficient cells (Fig. 5B). These data are thus consistent with a role of Tsa1 in modulating PKA activity downstream of cAMP.

The lethality *of ras1Δras2Δ* double mutants can be rescued by genetic interventions that restore PKA activity downstream of Ras, i.e. the inactivation of Pde2 or of the PKA negative regulatory subunit Bcy1 (Garrett & Broach, 1989; Toda et al., 1985; Wilson & Tatchell, 1988), or of Yak1, which is also downstream of PKA. Loss of Msn2 alone or of both Msn2 and its homologue Msn4, can also partially overcome the growth impairment of the partial loss of active Ras (Fig. 3C) and the requirement for a PKA catalytic subunit-encoding (*TPK*)-gene for viability (Smith, Ward, & Garrett, 1998). To test whether loss of Tsa1 could similarly compensate for the lack of Ras proteins we sporulated heterozygous *ras1Δ/RAS1*, *ras2Δ/RAS2* and *tsa1Δ/TSA1* diploid cells. Among the wild-type and single mutant spores only the absence of *RAS2* conferred a moderately increased spore lethality (3 out of 18 spores or 17%, Fig. 5C) consistent with the significantly reduced PKA activity of such cells. The increased spore lethality in Ras2-deficient cells seemed to be in part mediated by Tsa1, since none of the 20 *ras2Δtsa1Δ* spores died, suggesting that Tsa1 also affected spore germination downstream of Ras. Importantly, however, lack of Tsa1 was unable to bypass the requirement for either Ras1 or Ras2 in spore germination, since no cells lacking both Ras1 and Ras2 were viable irrespective of the presence or absence of Tsa1 (Fig. 5C). Along similar lines, lack of Tsa1 counteracted the moderately increased spore lethality of cells lacking the *TPK2* and/or *TPK3* genes encoding PKA catalytic subunits (Fig. S3A), but could not overcome the requirement of a single PKA catalytic subunit for spore germination (Toda, Cameron, Sass, Zoller, & Wigler, 1987). We indeed did not obtain viable *tsa1Δ tpk1Δ tpk2Δ tpk3Δ* spores in a cross between haploid *tsa1Δ* and *tpk1Δ tpk2Δ tpk3Δ* strains unless a centromeric *TPK1* plasmid, used to keep the *tpk1Δ tpk2Δ tpk3Δ* strain alive, was also present (in 6 out of 6 viable spores with the genomic *tsa1Δ tpk1Δ tpk2Δ tpk3Δ* genotype, Fig. S3A).

In addition, we noted that overproduction of the PKA negative regulatory subunit (mc-*BCY1*) could not overcome the PKA signaling defect in Tsa1-deficient cells, although dramatically increasing the Msn2 response to H_2O_2 in Tsa1-proficient cells (Fig. 5D).

Taken together the data indicate that Tsa1 affects PKA downstream of the second messenger cAMP.

Tpk1 is glutathionylated on the conserved Cys243

The above data indicate that Tsa1 suppresses PKA activity potentially by the intermediacy of both thioredoxins. Since this could be occurring through a redox-based mechanism we probed the effect of H_2O_2 on the redox-state of Bcy1 and Tpk1 cysteine residues in Tsa1- or thioredoxin-deficient cells and in cells expressing Tsa1- or thioredoxin 'cysteine-trap' mutants (*tsa1C171S or trx2C34S,* respectively). We chose Tpk1 as it is the most highly expressed of the three PKA catalytic subunits. Neither Bcy1 nor Tpk1 displayed any redox-dependent change of electrophoretic mobility under non-reducing conditions (Fig. S3B-D). To search for Tpk1 post-translational modifications (PTMs), we undertook mass spectrometric analysis of tagged, affinity-purified His- and biotin-tagged Tpk1 (Tpk1-HB, (Tagwerker et al., 2006)). We searched both for known PTMs, i.e. oxidation, sulfinylation, glutathionylation and phosphorylation, and, via an unbiased open search approach, unknown PTMs (Supplemental Table S1, Fig. S3E-F). We then selected a set of peptides covering the most abundant Tpk1 PTMs and performed a quantitative analysis that employs label free quantification of MS1 peaks, followed by a targeted MS/MS approach applying parallel reaction monitoring (PRM). We found that Tpk1Cys195 (Fig. S3G, Supplementary data Table S2) peptide was glutathionylated (-S-SG), in cells prior to exposure to H_2O_2. Label-free quantification and PRM suggested that the levels

of all three peptides bearing glutathionylated Cys195 decreased by 6 and 11-fold upon cell exposure to 0.4 mM and 0.8 mM H_2O_2, respectively, suggesting that this peptide undergoes one or more unknown modifications in response to H_2O_2 (Fig. S3G, Supplemental Tables S3 and S4).

Tpk1Cys243 containing peptides were also found heavily modified prior to H_2O_2 exposure, with the presence of various combinations of Cys243 reduced (-SH), glutathionylated and sulfinylated (SO_2H) forms, and of Thr241 bearing a phosphate group (Fig. 5F, Fig. S3F, S3H, Supplemental Table S2). The PRM signals of glutathionylated and non-glutathionylated peptides were of the same magnitude, suggesting that a significant fraction of Tpk1 is constitutively glutathionylated (Fig. 5F, Supplementary Table S4). This proportion may decrease upon H_2O_2 addition, since the levels of the Thr241-phosphorylated and Cys243 glutathionylated peptide decreased 2.5-fold, whereas the Thr241 unmodified Cys243 glutathionylated only barely changed upon H_2O_2 treatment (1.4-fold increase, Fig. 5F).

To further document redox modification of Tpk1, we used the PEG-maleimide assay in which oxidized cysteines are alkylated by PEG-maleimide, whereas, reduced cysteines are alkylated by N-ethylmaleimide (NEM) adding 5 kDa of molecular weight per oxidized cysteine. We observed that in addition to Tpk1, that migrated at the expected size of 50 kDa, another Tpk1 immunoreactive band of slower mobility was present prior to H_2O_2 exposure, the intensity of which increased after exposure to the oxidant (Fig. 5G). This H_2O_2-inducible, mPEG-reactive band could correspond to Tpk1 glutathionylation or to any other reversible Tpk1 Cys residue redox modifications. To evaluate the contribution of Tpk1Cys243 in the formation of this band, we replaced this residue with an alanine (*tpk1C243A tpk2Δ tpk3Δ*), and found that this band was still present, but no longer increased in intensity upon H_2O_2 addition (Fig. S3I).

We conclude from these results that Tpk1 is glutathionylated on Cys195 and Cys243, the amount of both which decreases upon exposure to H_2O_2, and, in addition, that Tpk1 is phosphorylated at Thr241. In addition, Tpk1 undergoes further redox modification upon H_2O_2 addition which targets the conserved Cys243.

A Tpk1 homology models suggests that Cys243 glutathionylation decreases PKA activity

In the mouse type II catalytic subunit, glutathionylation of Cys199, which is the residue homologous to Tpk1Cys243, reduces kinase activity *in vitro* by destabilizing the activation loop (Humphries, Deal, & Taylor, 2005; Huse & Kuriyan, 2002). We evaluated the effect of Cys243 glutathionylation by building a structural homology model of Tpk1, based on the mouse enzyme (Fig. 6A-B). Docking experiments suggested that Cys243-SSG stabilized the Thr241 dephosphorylated state by direct hydrogen bonding (Fig. 6C-E). Furthermore, in the presence of phosphorylated Thr241, glutathione moiety adopted a different position, now instead extending into the ATP binding pocket (Fig. 6C,F). Thr241 phosphorylation stabilizes the activation loop through hydrogen bonds to Arg209 and Lys233 (Fig. 6C-D). These data thus indicate that Cys243 glutathionylation and Thr241 phosphorylation have reciprocal negative influences on the enzyme, the former disfavoring and the latter favoring kinase activity by destabilizing or stabilizing the activation loop, respectively. In analogy to the *in vitro* mouse enzyme studies we found that increased Tpk1-Cys243 redox modification upon H_2O_2 addition (Fig. 5G, S3I) correlated with decreased levels of all three phosphorylated Tpk1-Thr241-peptides detected, and moderately increased levels of a non-phosphorylated Thr241 peptide (Fig. 5F, S3H).

Together with the quantitative MS data these results suggest that a significant proportion of Tpk1 molecules are inhibited by glutathionylation, dephoshorylation and destabilization of the activation loop in unstressed cells.

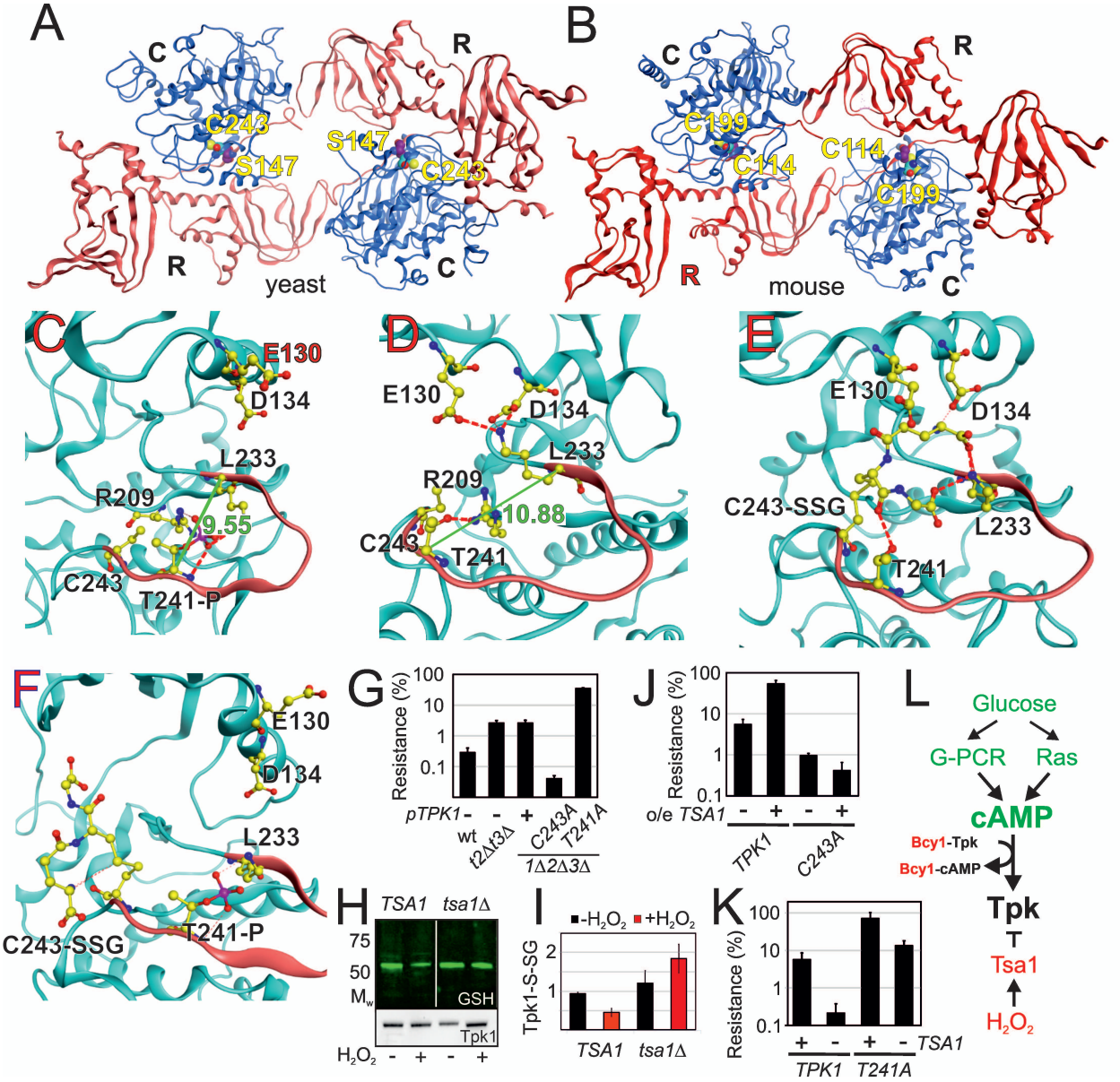

Figure 6. Tpk1 Cys243 redox-modification and Tsa1 inhibits PKA activity by dephosphorylating and destabilizing the activation loop. **A)** Homology model of the yeast holo-PKA enzyme consisting of two Tpk1 catalytic subunits (C) and two Bcy1 regulatory subunits (R). **B)** Structure of mouse type II PKA holoenzyme used to build the yeast structural homology model [PDB ID 3TNP, (P. Zhang et al., 2012)]. **C-F)** Amino acids in the activation loop (in red) of Tpk1 in the Thr241 phosphorylated Cys243 non-modified (**C**), Thr241 non-phosphorylated Cys243 non-modified (**D**), Thr241 non-modified Cys243 glutathionylated (**E**) and Thr241 phosphorylated Cys243 glutathionylated (**F**) states in the Tpk1 structural homology model. The backbones are colored in light blue, carbon atoms in yellow, nitrogen atoms in blue, oxygen atoms in red and phosphor atoms in scarlet. The distance between Lys233 and phosphorylated Thr241 is 9.55 Å (**c**) whereas Lys233 and non-phosphorylated Thr241 reside 10.88 Å apart (**D**). **G, J)** H_2O_2 resistance of the wild-type vector control (**G**, pRS313 or **J**, pRS403) or the indicated *TSA1*- or *tpk*-mutant strains. Strains in **J)** carry pRS316-*TPK1* or pRS316-*tpk1C243A* as the only PKA catalytic subunit (genomic *tpk1Δtpk2Δtpk3Δ* deletions, n=3). **H, I**) Glutathionylation of Tpk1-HB in *tpk2Δtpk3Δ (TSA1)* and *tpk2Δtpk3Δtsa1Δ (tsa1Δ)* as assayed by anti-glutathione immunoblot of immunoprecipitated Tpk1-HB in the absence of or 10 min following the addition of 0.4 mM H_2O_2. Extracts were separated under non-reducing (NR) or reducing (R) conditions. **J)** H_2O_2 resistance of *tpk1Δtpk2Δtpk3Δ* and *tpk1Δtpk2Δtpk3Δtsa1Δ* cells transformed with pRS313-*TPK1* or pRS313-*tpk1T241A* as indicated (n=3). **K)** Overview of mechanisms by which glucose and H_2O_2 impinge on PKA activity. In green activators and in red inhibitors.

Tpk1 Cys243 glutathionylation and dephosphorylation of the activation loop of PKA increases H_2O_2 resistance

To assess the physiological impact of the modified Tpk1 Cys195 and Cys243, we tested the effect of alanine substitution of these residues in cells expressing *TPK1* as the only catalytic subunit (*tpk2Δtpk3Δ*). Both these mutants supported a normal growth (Fig. S4A-C) but, interestingly *tpk1C243A*, but not *tpk1C195A*, substitution rendered cells hyper-sensitive to H_2O_2 (Fig. 6G, S4D). This corroborates the notion that Tpk1 cysteine 243 glutathionylation represses PKA activity, which is needed for H_2O_2 resistance.

We also assayed the phenotypes of *tpk1T241A* mutation in otherwise Tpk2 and Tpk3-lacking cells, since phosphorylation of this residue decreased upon exposure to H_2O_2. Whereas *tpk1T241A* mutant cells grew at normal rates (Fig. S4A-C) they were resistant to H_2O_2 (Fig. 6G), in keeping with the idea that reduced phosphorylation of Thr241 moderately decreases PKA activity and makes cells resistant to H_2O_2.

Tsa1-mediated H_2O_2 resistance requires Tpk1C243 and the destabilization of the Tpk1 activation loop

We next sought to evaluate the link between Tsa1 and Tpk1 glutathionylation by immunoprecipitating Tpk1-HB from Tsa1-proficient and –deficient cells and assayed glutathionylation by anti-glutathione immunoblot (Fig. 6H-I). Whereas Tpk1 glutathionylation seemed unaffected in the Tsa1-mutant in the absence of H_2O_2, the decreased Tpk1 glutathionylation seen in the wild-type was lost, suggesting a key role of Tsa1 in Tpk1 redox status upon H_2O_2 addition.

To evaluate the importance of Tpk1C243 in Tsa1-mediated H_2O_2 resistance we assayed the H_2O_2 resistance of *TSA1/TSA1* merodiploid and *TSA1*/vector control cells expressing *TPK1* or *tpk1C243A* as the sole PKA catalytic subunits. Interestingly, in support for a crucial role of C243-dependent redox modification in Tsa1-mediated H_2O_2 resistance, Tpk1C243 was essential for the H_2O_2 resistance conferred by an extra copy of the *TSA1* gene (Fig. 6J).

Finally, we sought to evaluate whether dephosphorylation of the activation loop in the catalytic subunit of PKA contributed to Tsa1-dependent H_2O_2 resistance. To this end, we expressed the *tpk1T241A* allele as the sole catalytic subunit in cells lacking Tsa1 and assessed H_2O_2 resistance. In support of a crucial role for dephosphorylation of the Tpk1 activation loop in Tsa1-mediated H_2O_2 resistance the *tpk1T241A* allele was able to partly overcome the H_2O_2 sensitivity of *tsa1Δ* cells (Fig. 6K).

We conclude that the dominant cytosolic yeast peroxiredoxin Tsa1 impacts on H_2O_2 resistance via a mechanism involving redox modulation of a conserved cysteine in and dephosphorylation of the activation loop in the catalytic subunit of protein kinase A.

Discussion

The ability of caloric restriction to extend the lifespan of organisms from yeast to primates has attracted much attention in the aging field. Since the incidence of many major age-related diseases such as cancer, diabetes and neurodegeneration is also reduced upon caloric restriction (Mattison et al., 2017), there is hope that reducing caloric intake or pharmaceutically targeting key molecular mechanisms underlying its beneficial health effects will fuel healthy, disease-free ageing.

There is widespread consensus in the aging-field that reduced nutrient and/or growth signaling through less than a handful of conserved pathways (e.g. insulin/IGF-1, TOR and protein kinase A) is instrumental for caloric restriction to slow down aging. In contrast, there is much more controversy regarding which downstream effector pathways/processes that are the most important in regulating the rate of aging. This could be a reflection of nutrient signaling coordinating the needs of many different cellular processes, the exact identity of which may differ slightly between different organisms and/or CR protocols (Lamming & Anderson, 2014). The fact that several of the target processes proposed (eg vacuolar pH control and protein homeostasis) reciprocally have been suggested to feed-back control nutrient signaling in themselves (Molin & Demir, 2014; Yao et al., 2015; N. Zhang, Quan, Rash, & Oliver, 2013) has caused further controversy regarding which mechanisms are most important in slowing down aging. A modern integrative model of aging, however, posits that different pathways and/or organelles are intricately interconnected into so called integrons. Interconnectivity allows the function of subsystems that fail to be compensated for by others, but also, conversely, that the failure of one subsystem can lead to the progressive decline of all systems through sequential collapse of homeostasis (Dillin, Gottschling, & Nystrom, 2014).

Peroxiredoxins have emerged as regulators of aging stimulating longevity in organisms from yeast to multicellulars such as worms, flies and mice (De Haes et al., 2014; Hanzen et al., 2016; Lee et al., 2009; Molin et al., 2011; Olahova & Veal, 2015). The fact that peroxiredoxins are conserved in organisms from bacteria to humans and that they can be targeted pharmaceutically to slow down aging suggests that they may constitute promising targets for the development of drugs against age-related disease.

We have previously shown that peroxiredoxin activity is crucial for molecular chaperones to bind to aggregates forming in aged yeast cells (Hanzen et al., 2016), thus connecting peroxiredoxins to an aging factor conserved in many organisms. We linked this role to the sulfinylation of the primary catalytic cysteine and enzyme double decamerisation, thus providing an *in vivo* function in a distinct chaperone network of this *in vitro* chaperone-active peroxiredoxin form (Jang et al., 2004; Noichri et al., 2015). However, we previously observed that H_2O_2 resistance in CR cells requires both catalytic cysteines (Molin et al., 2011). In addition, metformin leads to increased accumulation of disulfide-linked Prdx-2 in worms, raising the question of what the impact of peroxiredoxin catalytic cycling, or both the peroxidatic and resolving cysteines, on aging is. Data reported in this study demonstrate a key role of both cysteines of Tsa1 in slowing down aging, thus reinforcing the correlation between peroxiredoxin-stimulated longevity and hydrogen peroxide resistance. Surprisingly, however, the importance of the two peroxiredoxin catalytic cysteines in both aging and H_2O_2 resistance does not stem from a role in H_2O_2 scavenging. Taken together with the Tsa1-dependent increased lifespan in cells grown in the continuous presence of low levels of H_2O_2 (Goulev et al., 2017), these data clearly demonstrate that the anti-aging effect of peroxiredoxins originates in H_2O_2 signaling.

In this respect the key role of both Tsa1 catalytic cysteines in the regulation of the nutrient signaling enzyme PKA is highly interesting. By acting directly at the structurally highly conserved catalytic

subunits of protein kinases (Huse & Kuriyan, 2002), peroxiredoxins can override conventional second-messenger controlled upstream signaling mechanisms and directly modulate protein kinase signaling as a function of the level of H_2O_2 (Fig. 6L).

This idea is supported by our data suggesting a direct Tsa1-Tpk1 physical interaction and a requirement for Cys243 in H_2O_2 resistance mediated by mild Tsa1 overexpression. Our data suggest a model in which a significant proportion of the PKA catalytic subunit molecules are glutathionylated *in vivo*. The decreased ability of *tpk1C243A* mutant cells to resist H_2O_2 reflects enzyme hyperactivity and PKA signaling normally being restrained by glutathionylation. The homologous cysteine in murine type II PKA (Cys199) has previously been shown to be inactivated upon *in vitro* glutathionylation (Humphries et al., 2005; Humphries, Juliano, & Taylor, 2002). In addition, the homologous cysteine in type II rat PKA forms a disulfide bond with the regulatory subunit (de Pina et al., 2008). Intersubunit disulfide bond formation decreased PKA activity already at very low levels of H_2O_2 *in vitro* (1 μM) highlighting the importance of this cysteine in oxidative PKA regulation. However, the cysteine in the regulatory subunit is only conserved in vertebrates. In contrast, the catalytic subunit cysteine is conserved in PKA across eukaryotes (de Pina et al., 2008) suggesting that redox-modification of the catalytic subunit is the more conserved mechanism of oxidative PKA control. In addition, whereas intersubunit disulfide formation locks the enzyme in an inactive state our data indicate that destabilization of the substrate binding activation loop represents a more subtle regulatory mechanism to fine-tune PKA activity upon H_2O_2 addition (Fig. 6G, S4C). A pressing question for the future will be to identify the specific peroxiredoxin-mediated cysteine modification reducing PKA activity upon H_2O_2 addition.

Interestingly, other studies have reported that the activities of both protein kinase G and A are stimulated by H_2O_2 (Burgoyne et al., 2007; Burgoyne et al., 2015). Specifically, the I alpha isoform of protein kinase G in rat cells, PKGIalpha, formed a disulfide linking its two subunits in cells exposed to exogenous H_2O_2, which activated the enzyme (Burgoyne et al., 2007). Thus the regulation of PKA/PKG by H_2O_2 involves the same conserved cysteine in the catalytic subunit but leads to opposite effects. In a similar fashion *in vitro* studies suggest that the energy-sensing kinase AMPK is activated upon glutathionylation (Klaus et al., 2013). Thus the impact of oxidants on protein kinases seems to be different for different kinases.

In worms and mammals, the endoplasmic reticulum (ER) transmembrane kinase Ire-1 is regulated by oxidation of another conserved Cys residue in the activation loop, situated 11 residues upstream of the here described PKA cysteine, at position +2 relative to the Mg^{2+}-coordinating DFG motif (Hourihan, Moronetti Mazzeo, Fernandez-Cardenas, & Blackwell, 2016). Ire-1 was shown to be sulfenylated by ER and mitochondrial H_2O_2, as well as H_2O_2 produced by an NADPH oxidase in response to arsenite stress, in a manner activating the upstream mitogen activated protein kinase kinase kinase (MAPKKK) NSY-1 in the p38 stress-activated MAPK pathway. The switch between these two mutually exclusive functions of IRE-1 mediated by the sulfenylation of a unique cysteine residue supports the idea of cysteine oxidation being able to profoundly alter protein kinase function.

In summary data presented here and in a previous study (Hanzen et al., 2016) point to two different mechanisms by which peroxiredoxins counteract aging and age-related disease (Fig. 7), one involving catalytic cycling and the inhibition of nutrient-related kinase signaling (Fig. 7A-B). This mechanism appears to be critical for yeast to sustain normal longevity and is probably involved also in the ability of CR to slow down aging, since CR stimulated H_2O_2 resistance in a manner dependent on Tsa1

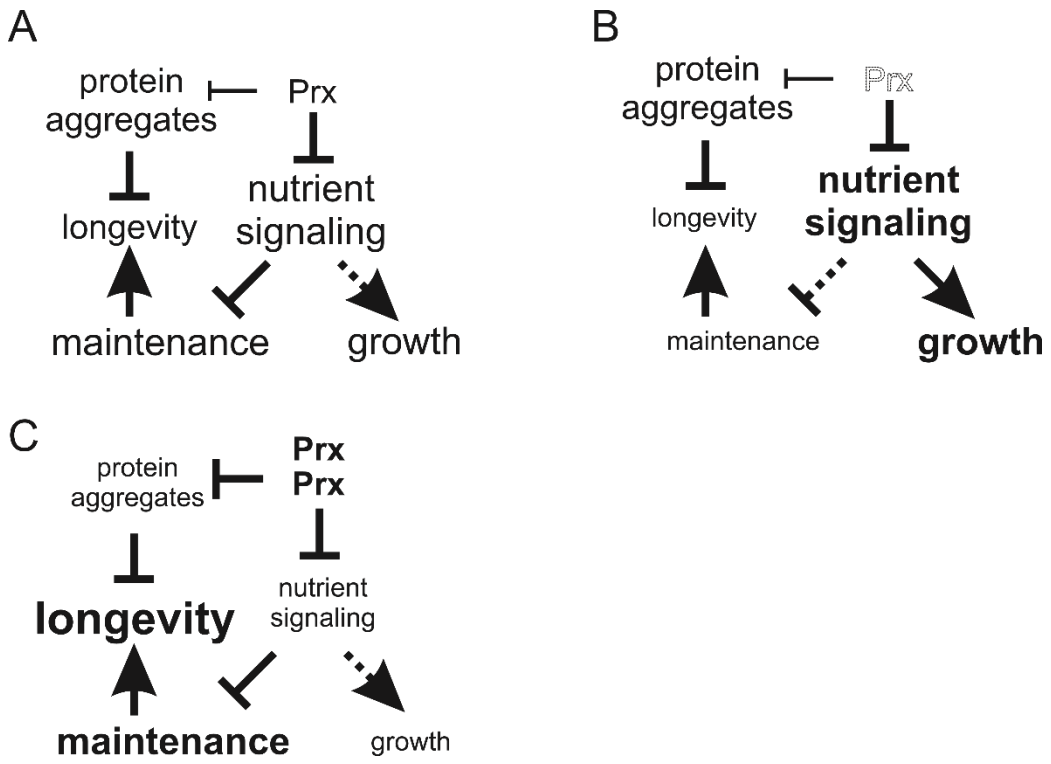

Figure 7. Model of the mechanisms by which altered peroxiredoxin levels impacts on aging. In the first mechanism peroxiredoxin-dependent redox-signaling impacts in an unconventional manner on the PKA nutrient signaling kinase (this study) and in the other on proteostasis (Hanzen et al., 2016). **A)** In wild-type cells Tsa1 catalytic cycling maintains longevity by decreasing PKA-dependent nutrient signaling leading to the stimulation of maintenance but at the expense of growth. **B)** In contrast, in cells lacking Tsa1 nutrient signaling is aberrantly increased leading to reduced maintenance and increased growth. **C)** Enforced expression of the peroxiredoxin Tsa1 slows down aging both by repressing nutrient signaling (this study) and by stimulating protein quality control mechanisms to reduce the levels of damaged and aggregated protein (Hanzen et al., 2016).

(Hanzen et al., 2016)catalytic cycling (Molin et al., 2011). Along the same lines, metformin-stimulated longevity in worms also seems to involve increased Prdx-2 catalytic cycling (De Haes et al., 2014). The second mechanism by which peroxiredoxins may inhibit aging and age-related disease is by stimulating chaperone-dependent protein quality control to counteract protein aggregation [Fig. 7C, (Hanzen et al., 2016)]. In particular, we showed that Tsa1 sulfinylation was necessary to guide the molecular chaperones Hsp70 and Hsp104 to aggregates forming in aged and H_2O_2-treated cells. This anti-aging mechanism thus seems to be independent of the here described role in inhibiting nutrient signaling which instead appears to be linked to Tsa1 catalytic cycling. The requirement of both reduced PKA nutrient signaling (Pde2, this study) and normal protein quality control [e.g. cytosolic Hsp70 activity by Ssa1/2 (Hanzen et al., 2016)] for mild Tsa1 overproduction to extend lifespan support a requirement of both these mechanisms in the ability of enhanced peroxiredoxin levels to extend lifespan (Fig. 7C).

In the integrative view of aging, it can be assumed that a key role in the aging process is executed by cellular components and/or pathways that assimilate information from different subsystems such as the above described nutrient signaling pathways, the latter which would constitute excellent candidates of acting as such integrators. In agreement with a key role of PKA in yeast integrative homeostasis a genome-wide identification of genes controlling PKA regulatory-catalytic subunit interaction, and hence PKA activity, found a striking number of known targets of PKA, involved in eg glycogen

accumulation, filamentous growth and amino-acid biosynthesis (Filteau et al., 2015). Hence, the involvement of central nutrient signaling pathways in the mechanisms by which peroxiredoxins slow down aging is in agreement with the integrative model of aging and suggest that also other anti-aging regimens impact on nutrient signaling.

Acknowledgements

We are grateful to Michel B Toledano for valuable comments on the manuscript and Karin Voordeckers, Joseph Heitman and Robert J Deschenes for reagents. This work was supported by grants from the Swedish research Council VR, Cancerfonden, the Foundation Olle Engkvist byggmästare and Carl Tryggers stiftelse (all to MM).

Competing interests

The authors declare that they have no conflict of interest.

Author contributions

Conceptualization M.M.; Methodology M.M., W.R., M.H., C.G., N.W., J.L.; Investigation F.R., C.P., M.M., C.A., S.H., G.L.; Writing – Original Draft M.M., F.R.; Writing – Review and Editing, M.M., F.R., T.N., W.R., M.G.; Funding Acquisition M.M., M.H., T.N., M.G.; Supervision, M.M., M.G.

References

Abraham, M. J., Murtola, T., Schultz, R., Pall, S., Smith, J. C., Hess, B., & Lindahl, E. (2015). GROMACS: High performance molecular simulations through multi-level parallelism from laptops to supercomputers. *SoftwareX, 54*(7), 1932-1940.

Alic, N., & Partridge, L. (2011). Death and dessert: nutrient signalling pathways and ageing. *Curr Opin Cell Biol, 23*(6), 738-743. doi:10.1016/j.ceb.2011.07.006

Bilan, D. S., Pase, L., Joosen, L., Gorokhovatsky, A. Y., Ermakova, Y. G., Gadella, T. W. J., . . . Belousov, V. V. (2013). HyPer-3: A Genetically Encoded H2O2 Probe with Improved Performance for Ratiometric and Fluorescence Lifetime Imaging. *ACS chemical biology, 8*(3), 535-542. doi:10.1021/cb300625g

Biteau, B., Labarre, J., & Toledano, M. B. (2003). ATP-dependent reduction of cysteine-sulphinic acid by *S. cerevisiae* sulphiredoxin. *Nature, 425*(6961), 980-984.

Bodvard, K., Peeters, K., Roger, F., Romanov, N., Igbaria, A., Toledano, M. B., . . . Molin, M. (2017). Light-sensing via hydrogen peroxide and a peroxiredoxin. *Nat Commun, 8*, 14791. doi:10.1038/ncomms14791

Burgoyne, J. R., Madhani, M., Cuello, F., Charles, R. L., Brennan, J. P., Schroder, E., . . . Eaton, P. (2007). Cysteine redox sensor in PKGIa enables oxidant-induced activation. *Science, 317*(5843), 1393-1397. doi:10.1126/science.1144318

Burgoyne, J. R., Rudyk, O., Cho, H. J., Prysyazhna, O., Hathaway, N., Weeks, A., . . . Eaton, P. (2015). Deficient angiogenesis in redox-dead Cys17Ser PKARIalpha knock-in mice. *Nat Commun, 6*, 7920. doi:10.1038/ncomms8920

Colombo, S., & Martegani, E. (2014). Methods to study the Ras2 protein activation state and the subcellular localization of Ras-GTP in Saccharomyces cerevisiae. *Methods Mol Biol, 1120*, 391-405. doi:10.1007/978-1-62703-791-4_24

De Haes, W., Frooninckx, L., Van Assche, R., Smolders, A., Depuydt, G., Billen, J., . . . Temmerman, L. (2014). Metformin promotes lifespan through mitohormesis via the peroxiredoxin PRDX-2. *Proc Natl Acad Sci U S A, 111*(24), E2501-2509. doi:10.1073/pnas.1321776111

de Pina, M. Z., Vazquez-Meza, H., Pardo, J. P., Rendon, J. L., Villalobos-Molina, R., Riveros-Rosas, H., & Pina, E. (2008). Signaling the signal, cyclic AMP-dependent protein kinase inhibition by insulin-formed H2O2 and reactivation by thioredoxin. *J Biol Chem, 283*(18), 12373-12386. doi:10.1074/jbc.M706832200

Dillin, A., Gottschling, D. E., & Nystrom, T. (2014). The good and the bad of being connected: the integrons of aging. *Curr Opin Cell Biol, 26*, 107-112. doi:10.1016/j.ceb.2013.12.003

Filteau, M., Diss, G., Torres-Quiroz, F., Dube, A. K., Schraffl, A., Bachmann, V. A., . . . Landry, C. R. (2015). Systematic identification of signal integration by protein kinase A. *Proc Natl Acad Sci U S A, 112*(14), 4501-4506. doi:10.1073/pnas.1409938112

Fontan-Lozano, A., Lopez-Lluch, G., Delgado-Garcia, J. M., Navas, P., & Carrion, A. M. (2008). Molecular bases of caloric restriction regulation of neuronal synaptic plasticity. *Mol Neurobiol, 38*(2), 167-177.

Fontana, L., Partridge, L., & Longo, V. D. (2010). Extending healthy life span--from yeast to humans. *Science, 328*(5976), 321-326. doi:10.1126/science.1172539

Fontana, L., Partridge, L., and Longo, V.D. (2010). Dietary Restriction, Growth Factors and Aging: from yeast to humans. *Science, 328*(5679), 321-326.

Garrett, S., & Broach, J. (1989). Loss of Ras activity in Saccharomyces cerevisiae is suppressed by disruptions of a new kinase gene, YAKI, whose product may act downstream of the cAMP-dependent protein kinase. *Genes Dev, 3*(9), 1336-1348.

Goulev, Y., Morlot, S., Matifas, A., Huang, B., Molin, M., Toledano, M., & Charvin, G. (2017). Nonlinear feedback drives homeostatic plasticity in H2O2 stress response. *Elife, 6*, 23791. doi:http://dx.doi.org/10.7554/eLife.23971

Hanzen, S., Vielfort, K., Yang, J., Roger, F., Andersson, V., Zamarbide-Fores, S., . . . Nystrom, T. (2016). Lifespan Control by Redox-Dependent Recruitment of Chaperones to Misfolded Proteins. *Cell, 166*(1), 140-151. doi:10.1016/j.cell.2016.05.006

Heilbronn, L. K., de Jonge, L., Frisard, M. I., DeLany, J. P., Larson-Meyer, D. E., Rood, J., . . . Pennington, C. T. (2006). Effect of 6-month calorie restriction on biomarkers of longevity, metabolic adaptation, and oxidative stress in overweight individuals: a randomized controlled trial. *JAMA, 295*(13), 1539-1548. doi:10.1001/jama.295.13.1539

Hourihan, J. M., Moronetti Mazzeo, L. E., Fernandez-Cardenas, L. P., & Blackwell, T. K. (2016). Cysteine Sulfenylation Directs IRE-1 to Activate the SKN-1/Nrf2 Antioxidant Response. *Mol Cell, 63*(4), 553-566. doi:10.1016/j.molcel.2016.07.019

Humphries, K. M., Deal, M. S., & Taylor, S. S. (2005). Enhanced dephosphorylation of cAMP-dependent protein kinase by oxidation and thiol modification. *J Biol Chem, 280*(4), 2750-2758. doi:10.1074/jbc.M410242200

Humphries, K. M., Juliano, C., & Taylor, S. S. (2002). Regulation of cAMP-dependent protein kinase activity by glutathionylation. *J Biol Chem, 277*(45), 43505-43511. doi:10.1074/jbc.M207088200

Huse, M., & Kuriyan, J. (2002). The conformational plasticity of protein kinases. *Cell, 109*(3), 275-282.

Jacobson, M. P., Friesner, R. A., Xiang, Z., & Honig, B. (2002). On the role of the crystal environment in determining protein side-chain conformations. *J Mol Biol, 320*(3), 597-608.

Jang, H. H., Lee, K. O., Chi, Y. H., Jung, B. G., Park, S. K., Park, J. H., . . . Lee, S. Y. (2004). Two enzymes in one; two yeast peroxiredoxins display oxidative stress-dependent switching from a peroxidase to a molecular chaperone function. *Cell, 117*(5), 625-635.

Kenyon, C. J. (2010). The genetics of ageing. *Nature, 464*(7288), 504-512. doi:nature08980 [pii] 10.1038/nature08980

Klaus, A., Zorman, S., Berthier, A., Polge, C., Ramirez, S., Michelland, S., . . . Schlattner, U. (2013). Glutathione S-transferases interact with AMP-activated protein kinase: evidence for S-

glutathionylation and activation in vitro. *PLoS One, 8*(5), e62497. doi:10.1371/journal.pone.0062497

Kong, A. T., Leprevost, F. V., Avtonomov, D. M., Mellacheruvu, D., & Nesvizhskii, A. I. (2017). MSFragger: ultrafast and comprehensive peptide identification in mass spectrometry-based proteomics. *Nat Methods, 14*(5), 513-520. doi:10.1038/nmeth.4256

Lamming, D. W., & Anderson, R. M. (2014). Metabolic Effects of Caloric Restriction. In *eLS*: John Wiley & Sons, Ltd.

Lee, K. S., Iijima-Ando, K., Iijima, K., Lee, W. J., Lee, J. H., Yu, K., & Lee, D. S. (2009). JNK/FOXO-mediated neuronal expression of fly homologue of peroxiredoxin II reduces oxidative stress and extends life span. *J Biol Chem, 284*(43), 29454-29461. doi:M109.028027 [pii] 10.1074/jbc.M109.028027

Leichert, L. I., & Dick, T. P. (2015). Incidence and physiological relevance of protein thiol switches. *Biol Chem, 396*(5), 389-399. doi:10.1515/hsz-2014-0314

Lin, S. J., Defossez, P. A., & Guarente, L. (2000). Requirement of NAD and SIR2 for life-span extension by calorie restriction in Saccharomyces cerevisiae. *Science, 289*(5487), 2126-2128.

Longo, V. D., Shadel, G. S., Kaeberlein, M., & Kennedy, B. (2012). Replicative and chronological aging in Saccharomyces cerevisiae. *Cell metabolism, 16*(1), 18-31. doi:10.1016/j.cmet.2012.06.002

Mashhoon, N., Carmel, G., Pflugrath, J. W., & Kuret, J. (2001). Structure of the unliganded cAMP-dependent protein kinase catalytic subunit from Saccharomyces cerevisiae. *Arch Biochem Biophys, 387*(1), 11-19. doi:10.1006/abbi.2000.2241

Mattison, J. A., Colman, R. J., Beasley, T. M., Allison, D. B., Kemnitz, J. W., Roth, G. S., . . . Anderson, R. M. (2017). Caloric restriction improves health and survival of rhesus monkeys. *Nat Commun, 8*, 14063. doi:10.1038/ncomms14063

Molin, M., & Demir, A. B. (2014). Linking Peroxiredoxin and Vacuolar-ATPase Functions in Calorie Restriction-Mediated Life Span Extension. *Int J Cell Biol, 2014*, 12. doi:10.1155/2014/913071

Molin, M., Yang, J., Hanzen, S., Toledano, M. B., Labarre, J., & Nystrom, T. (2011). Life span extension and H_2O_2-resistance elicited by caloric restriction require the peroxiredoxin Tsa1 in *Saccharomyces cerevisiae*. *Mol Cell, 43*(5), 823-833. doi:10.1016/j.molcel.2011.07.027

Neumann, C. A., Krause, D. S., Carman, C. V., Das, S., Dubey, D. P., Abraham, J. L., . . . Van Etten, R. A. (2003). Essential role for the peroxiredoxin Prdx1 in erythrocyte antioxidant defence and tumour suppression. *Nature, 424*(6948), 561-565.

Noichri, Y., Palais, G., Ruby, V., D'Autreaux, B., Delaunay-Moisan, A., Nystrom, T., . . . Toledano, M. B. (2015). In vivo parameters influencing 2-Cys Prx oligomerization: The role of enzyme sulfinylation. *Redox Biol, 6*, 326-333. doi:10.1016/j.redox.2015.08.011

Nystrom, T., Yang, J., & Molin, M. (2012). Peroxiredoxins, gerontogenes linking aging to genome instability and cancer. *Genes Dev, 26*(18), 2001-2008. doi:10.1101/gad.200006.112

Olahova, M., & Veal, E. A. (2015). A peroxiredoxin, PRDX-2, is required for insulin secretion and insulin/IIS-dependent regulation of stress resistance and longevity. *Aging Cell, 14*(4), 558-568. doi:10.1111/acel.12321

Peeters, K., Van Leemputte, F., Fischer, B., Bonini, B. M., Quezada, H., Tsytlonok, M., . . . Thevelein, J. M. (2017). Fructose-1,6-bisphosphate couples glycolytic flux to activation of Ras. *Nat Commun, 8*(1), 922. doi:10.1038/s41467-017-01019-z

Ponder, J. W., & Case, D. A. (2003). Force fields for protein simulations. *Adv Protein Chem, 66*, 27-85.

Rappsilber, J., Mann, M., & Ishihama, Y. (2007). Protocol for micro-purification, enrichment, pre-fractionation and storage of peptides for proteomics using StageTips. *Nat Protoc, 2*(8), 1896-1906. doi:10.1038/nprot.2007.261

Reiter, W., Anrather, D., Dohnal, I., Pichler, P., Veis, J., Grotli, M., . . . Ammerer, G. (2012). Validation of regulated protein phosphorylation events in yeast by quantitative mass spectrometry analysis of purified proteins. *Proteomics, 12*(19-20), 3030-3043. doi:10.1002/pmic.201200185

Santangelo, G. M. (2006). Glucose signaling in *Saccharomyces cerevisiae*. *Microbiol Mol Biol Rev, 70*(1), 253-282.

Schulz, T. J., Zarse, K., Voigt, A., Urban, N., Birringer, M., & Ristow, M. (2007). Glucose restriction extends Caenorhabditis elegans life span by inducing mitochondrial respiration and increasing oxidative stress. *Cell metabolism, 6*(4), 280-293. doi:10.1016/j.cmet.2007.08.011

Smith, A., Ward, M. P., & Garrett, S. (1998). Yeast PKA represses Msn2p/Msn4p-dependent gene expression to regulate growth, stress response and glycogen accumulation. *Embo J, 17*(13), 3556-3564.

Sohal, R. S., & Forster, M. J. (2014). Caloric restriction and the aging process: a critique. *Free Radic Biol Med, 73*, 366-382. doi:10.1016/j.freeradbiomed.2014.05.015

Stocker, S., Van Laer, K., Mijuskovic, A., & Dick, T. P. (2017). The Conundrum of Hydrogen Peroxide Signaling and the Emerging Role of Peroxiredoxins as Redox Relay Hubs. *Antioxid Redox Signal*. doi:10.1089/ars.2017.7162

Sun, J., Kale, S. P., Childress, A. M., Pinswasdi, C., & Jazwinski, S. M. (1994). Divergent roles of RAS1 and RAS2 in yeast longevity. *J Biol Chem, 269*(28), 18638-18645.

Tagwerker, C., Flick, K., Cui, M., Guerrero, C., Dou, Y., Auer, B., . . . Kaiser, P. (2006). A tandem affinity tag for two-step purification under fully denaturing conditions: application in ubiquitin profiling and protein complex identification combined with in vivocross-linking. *Mol Cell Proteomics, 5*(4), 737-748. doi:10.1074/mcp.M500368-MCP200

Toda, T., Cameron, S., Sass, P., Zoller, M., & Wigler, M. (1987). Three different genes in S. cerevisiae encode the catalytic subunits of the cAMP-dependent protein kinase. *Cell, 50*(2), 277-287. doi:0092-8674(87)90223-6 [pii]

Toda, T., Uno, I., Ishikawa, T., Powers, S., Kataoka, T., Broek, D., . . . Wigler, M. (1985). In yeast, RAS proteins are controlling elements of adenylate cyclase. *Cell, 40*(1), 27-36.

Wilson, R. B., & Tatchell, K. (1988). SRA5 encodes the low-Km cyclic AMP phosphodiesterase of Saccharomyces cerevisiae. *Mol Cell Biol, 8*(1), 505-510.

Vizcaino, J. A., Csordas, A., del-Toro, N., Dianes, J. A., Griss, J., Lavidas, I., . . . Hermjakob, H. (2016). 2016 update of the PRIDE database and its related tools. *Nucleic Acids Res, 44*(D1), D447-456. doi:10.1093/nar/gkv1145

Yao, Y., Tsuchiyama, S., Yang, C., Bulteau, A. L., He, C., Robison, B., . . . Schmidt, M. (2015). Proteasomes, Sir2, and Hxk2 form an interconnected aging network that impinges on the AMPK/Snf1-regulated transcriptional repressor Mig1. *PLoS Genet, 11*(1), e1004968. doi:10.1371/journal.pgen.1004968

Zhang, N., Quan, Z., Rash, B., & Oliver, S. G. (2013). Synergistic effects of TOR and proteasome pathways on the yeast transcriptome and cell growth. *Open Biol, 3*(5), 120137. doi:10.1098/rsob.120137

Zhang, P., Smith-Nguyen, E. V., Keshwani, M. M., Deal, M. S., Kornev, A. P., & Taylor, S. S. (2012). Structure and allostery of the PKA RIIbeta tetrameric holoenzyme. *Science, 335*(6069), 712-716. doi:10.1126/science.1213979

Zhu, K., Borrelli, K. W., Greenwood, J. R., Day, T., Abel, R., Farid, R. S., & Harder, E. (2014). Docking covalent inhibitors: a parameter free approach to pose prediction and scoring. *J Chem Inf Model, 54*(7), 1932-1940. doi:10.1021/ci500118s

Materials and methods

Detailed materials and methods can be found in Supplementary information.

Strains and growth conditions

Yeast strains and plasmids are listed in Supplementary Table S1. All the strains used in this study are derivatives of BY4741/BY4742. Strains were grown at 30°C in YPD 2% glucose (w/v) or in Yeast Nitrogen Base defined medium containing 2% glucose and complete supplement mixture (CSM) lacking the appropriate amino acids (Formedium) as described previously (Molin et al., 2011). Spot tests H2O2 spot tests

Global H_2O_2 scavenging in the medium

Medium peroxide determinations were performed using a ferrithiocyanate spectrophotometric assay (Molin et al., 2007).

Isolation of old cells

Old cells were obtained as previously described by sorting biotin-labeled mother cells using the MagnaBind streptavidin system (Sinclair and Guarente, 1997). After sorting the cells were imaged by microscopical analysis.

Measurements of cytoplasmic H_2O_2 using HyPer3

Fluorescence of the ratiometric probe HyPer-3 (Bilan et al., 2013) was acquired using an Olympus IX81 motorized microscope with a PlanApoN 60x/1.42 Oil objective and a 12-bit Hamamatsu camera. For bolus addition of H_2O_2, cells in midexponential phase were incubated with 0.2 mM H_2O_2 for 10 min and immediately imaged. Image and signal analysis was performed using the MATLAB toolbox 2016b. Cell segmentation is performed with the CellX algorithm using the bright-field channel.

Lifespan Analyses

Lifespan analyses were performed as previously described by counting the number of daughters produced in a cohort of mother cells (Erjavec et al., 2007).

Quantitative Real-Time PCR Analysis

Cell were lysed using Trizol Reagent (Invitrogen) upon cell homogenization with silica beads by Fast prep (6.5 m/s, 30 sec, interval 2.5min, 4 ◦C). RNA was extracted using phenol chloroform extraction, purified with Invitrogen PureLink RNA Mini Kit columns and converted to cDNA using the QIAGEN QuantiTect Reverse Transcription Kit. Q-PCR was performed using the BioRad iQ SYBR Green Supermix and quantified with the BioRad iCycler, iQ5. *ACT1* was used as a reference gene.

2D-PAGE

Protein synthesis rates of the indicated proteins were determined in ^{35}S-Methionine labelled protein extracts separated by two-dimensional polyacrylamide gel electrophoresis as described (Maillet et al., 1996; Molin et al., 2011).

Measurement of Ras2-GTP *in vivo*

Ras2-GTP level were measured as a ratio between Ras2-GTP and total Ras2 as described previously (Colombo & Martegani, 2014; Peeters et al., 2017).

cAMP measurement

cAMP measurements were performed as previously described (Caballero et al., 2011; Parts et al., 2011).

Spore viability

The viability of spores segregating in the sporulation and dissection of a heterozygous diploid strains were analyzed after 4 days of incubation at 30˚C by in tetrads where 1) all markers analyzed segregated 2:2, 2) the exact genotypes of all spores were possible to deduce from this information and 3) the genotypes of dead spores were assigned based on markers present in the other spores dissected from the same tetrads.

Immunoblot analysis

Immunoblot analysis of selected proteins was performed as described previously (Biteau, Labarre, & Toledano, 2003; Molin et al., 2011). Prior to separation on 12% Bis-Tris NuPAGE gels using an XCell SureLock MiniCell (Invitrogen) in NuPAGE MOPS running buffer as recommended by the supplier protein extracts were heated in Laemlii buffer (pH 8.7) either in the presence of β-mercaptoethanol (5%, reducing) or not (non-reducing) as indicated.

Glutathionylation of Tpk1 was assayed using anti-glutathione immunoblot on Tpk1-HB immunoprecipitated by Ni^{2+}-Sepharose beads following a protocol similar to that used during MS sample preparation (see below). We verified that the anti-glutathione immunoblot signal on immunoprecipitated Tpk1 completely disappeared upon extract reduction by β-mercaptoethanol.

Mass spectrometric sample preparation

Three independent experimental replicates were performed for each experimental condition. For HB (poly histidine, biotinylation signal) tandem affinity purifications were performed as described elsewhere (Reiter et al., 2012). Cleared extracts were incubated (4 hours, room temperature) with Ni^{2+}-Sepharose beads, washed with urea buffer and urea buffer pH 6.3. Proteins were eluted in urea buffer pH 4.3 containing 10mM EDTA, incubated overnight with streptavidin-agarose beads, washed using urea wash buffer containing 1% SDS and urea wash buffer without SDS. Beads were washed five times with 50 mM ammonium bicarbonate (ABC). Cys-residues were alkylated with IAA (25% w/w of the estimated amount of protein). Proteins were digested with trypsin at 37°C overnight. Digestion was stopped with trifluoroacetic acid (0.5% final concentration) and the peptides were desalted using C18 Stagetips (Rappsilber, Mann, & Ishihama, 2007).

Mass spectrometry analysis of Tpk1

Peptides were separated on an Ultimate 3000 RSLC nano-flow chromatography system (Thermo-Fisher), using a pre-column (Acclaim PepMap C_{18}, 2 cm × 0.1 mm, 5 µm, Thermo-Fisher), and a C_{18} analytical column (Acclaim PepMap C18, 50 cm × 0.75 mm, 2 µm, Thermo-Fisher). A Proxeon nanospray flex ion source (Thermo Fisher) using coated emitter tips (New Objective) was used for ionization. Peptides were analyzed on an Orbitrap Fusion Lumos Tribrid mass spectrometer (Thermo Fisher). MS proteomics data have been deposited to the ProteomeXchange Consortium through the

Proteomics Identifications database (PRIDE) partner repository (Vizcaino et al., 2016) with the data set identifiers PXD012617.

Closed database search

Peptide identification and label free quantification (LFQ) were performed using MaxQuant (version 1.6.0.16) with default parameters. N-terminal acetylation, deamidation of asparagine and glutamine, oxidation of methionine, tri-oxidation and glutathionylation of cysteine and phosphorylation of serine, threonine and tyrosine were set as variable protein modification. Carbamidomethylation of cysteine was set as fixed. A maximum of 5 variable modifications per peptide was allowed. A maximum of 2 missed cleavages per peptide was allowed. MaxLFQ (implemented in the MaxQuant package) was used for MS1-based label free quantification and normalization of protein groups.

Open search analysis of selected peptides

To screen for protein modifications in an unbiased manner we initially performed an open search using MSFragger in FragPipe (Kong, Leprevost, Avtonomov, Mellacheruvu, & Nesvizhskii, 2017). The default open search parameters were used, with trypsin specificity, +/- 500 Da windows and oxidation of methionine and carbamidomethylation of cysteine as variable modifications. The observed mass shifts were inspected and filtered for the most abundant and relevant modifications occurring in Tpk1.

Targeted mass-spectrometry

Parallel-Reaction-Monitoring (PRM) assays were generated based on the peptide information obtained by MaxQuant. We selected Tpk1 and Tsa1 peptides for targeted relative LFQ as specified in Supplementary Tables 4-6. Raw data were obtained on an Orbitrap Q Exactive HF-X (Thermo Fisher Scientific) mass spectrometer.

Data analysis, manual validation of all transitions (based on retention time, relative ion intensities, and mass accuracy), and relative quantification was performed in Skyline. Up to six characteristic transitions were selected for each peptide and their peak areas were summed for peptide quantification (total peak area). The mean of the log2 Tpk1 non-modified peptide intensities was used to normalize Tpk1 modified peptides and Tsa1 peptides to account for differences in Tpk1 levels. Tsa1 peptide intensities (anti-log) were summed up to obtain values for relative protein abundance.

mPEG assay

To assay oxidation of the Tpk1 protein we used a modified mPEG-switch assay (Burgoyne et al., 2013).

Quantitative analysis of Msn2 nuclear localization

The degree of nuclear localization of Msn2 upon the addition of H_2O_2 was analyzed in cells transformed with the pAMG plasmid on a Nikon TE2000E-PFS epi-fluorescence microscope at low light-intensity as described previously (Bodvard et al., 2017).

Homology modeling

A model of the yeast PKA tetramer structure was obtained by homology modeling. The protein sequences of yeast Tpk1 (catalytic subunit of PKA) and Bcy1 (regulatory subunit of PKA) were obtained from Genbank (ID: 1023942850 and ID: 1023943330, respectively). The crystal structure of

mouse PKA (PDBID: 3TNP) was used as the template for the homology calculations. The homology model was built using StructurePrediction panel (Jacobson, Friesner, Xiang, & Honig, 2002) in Schrödinger Suite (Schrödinger, LLC, New York, NY).

Covalent docking

Covalent docking was carried out to obtain a model for glutathionylated Tpk1. The Tpk1 crystal structure [PDB ID: 1FOT, (Mashhoon, Carmel, Pflugrath, & Kuret, 2001)] were prepared using the Protein Preparation utility in Schrodinger to assign the correct protonation state and fix the missing side chains and loops. The glutathione was built by 3D builder and prepared by LigPre utility in Schrodinger. The Covalent-Dock panel (Zhu et al., 2014) in Schrodinger was used to predict the pose of the glutathione attaching to Cys243. The reaction type was set to be disulfide formation, the docking mode was set to be thorough pose prediction, the other parameters were all set to be default. At the final step, Prime Energy was used to rank the poses of the ligand.

Molecular dynamics simulations

The GROMACS software (Abraham et al., 2015) was used for the Molecular dynamics simulations and the Amber 99 (Ponder & Case, 2003) force field was selected to assign the parameters for different amino acid residues. Glutathionylation and phosphorylation parameters were generated from Ambertools and incorporated into the GROMACS software.

Supplementary information

Peroxiredoxin promotes longevity and H_2O_2-resistance in yeast through redox-modulation of PKA

Friederike Roger, Cecilia Picazo, Chikako Asami, Wolfgang Reiter, Sarah Hanzén, Chunxia Gao, Gilles Lagniel, Niek Welkenhuysen, Jean Labarre, Thomas Nyström, Morten Grøtli, Markus Hartl and Mikael Molin

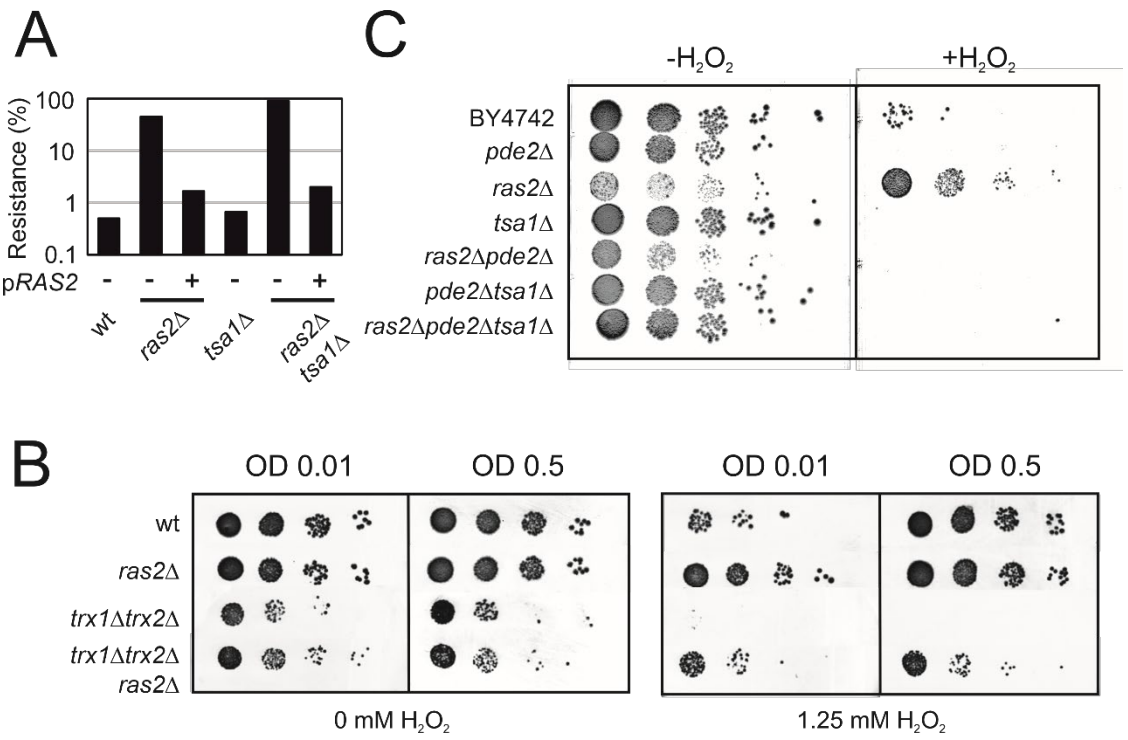

Figure S1. Related to Figure 2. Ras-deficiency counteracts the H_2O_2 sensitivity of cells lacking Tsa1 or the cytosolic thioredoxins Trx1 and Trx2 in a manner independent on increased H_2O_2 scavenging. **A)** H_2O_2 resistance in the indicated mutant strains complemented with a centromeric *RAS2* plasmid (pMW1, +) or transformed with the vector control plasmid (-, yCPlac33). **B-C)** H_2O_2 resistance in the indicated mutant strains strains grown to early (OD0.01) and mid exponential phase (OD0.5, **B**) or OD 0.3 (**C**) and spotted onto plates with or without the indicated amounts of H_2O_2.

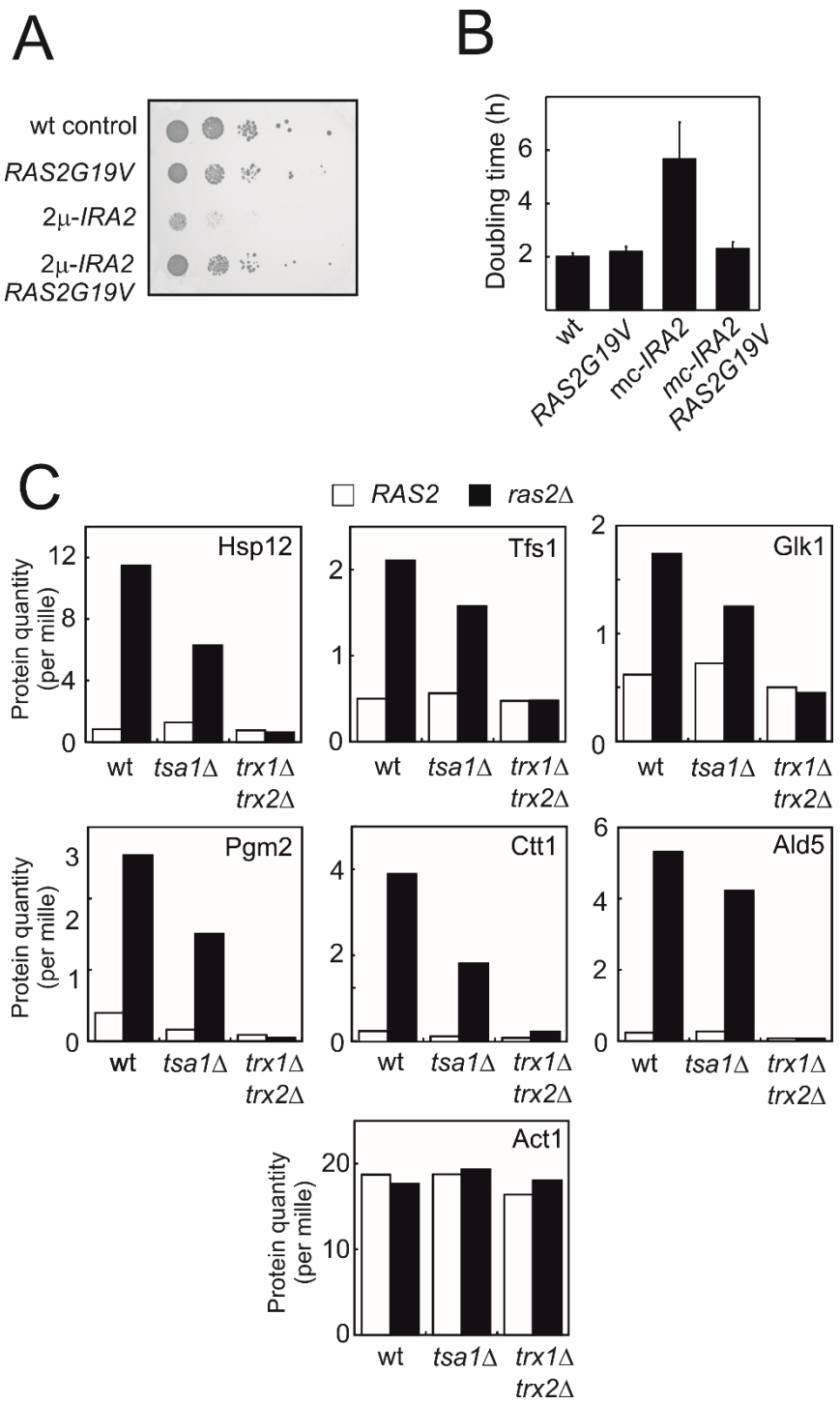

Figure S2. Related to Figure 3. Substantially reduced Ras activity slows down growth and activates Msn2 in a manner dependent on Tsa1 and the cytosolic thioredoxins. **A-B)** Growth of cells expressing the oncogenic *RAS2G19V* allele, overexpressing *IRA2* (mc-*IRA2*) or both. **C)** Expression of PKA repressed Msn2/4 targets (Hasan et al., 2002; Molin et al., 2011) in wild-type, *tsa1Δ* or *trx1Δtrx2Δ* cells deficient in *RAS2* (*ras2Δ*) or not (*RAS2*).

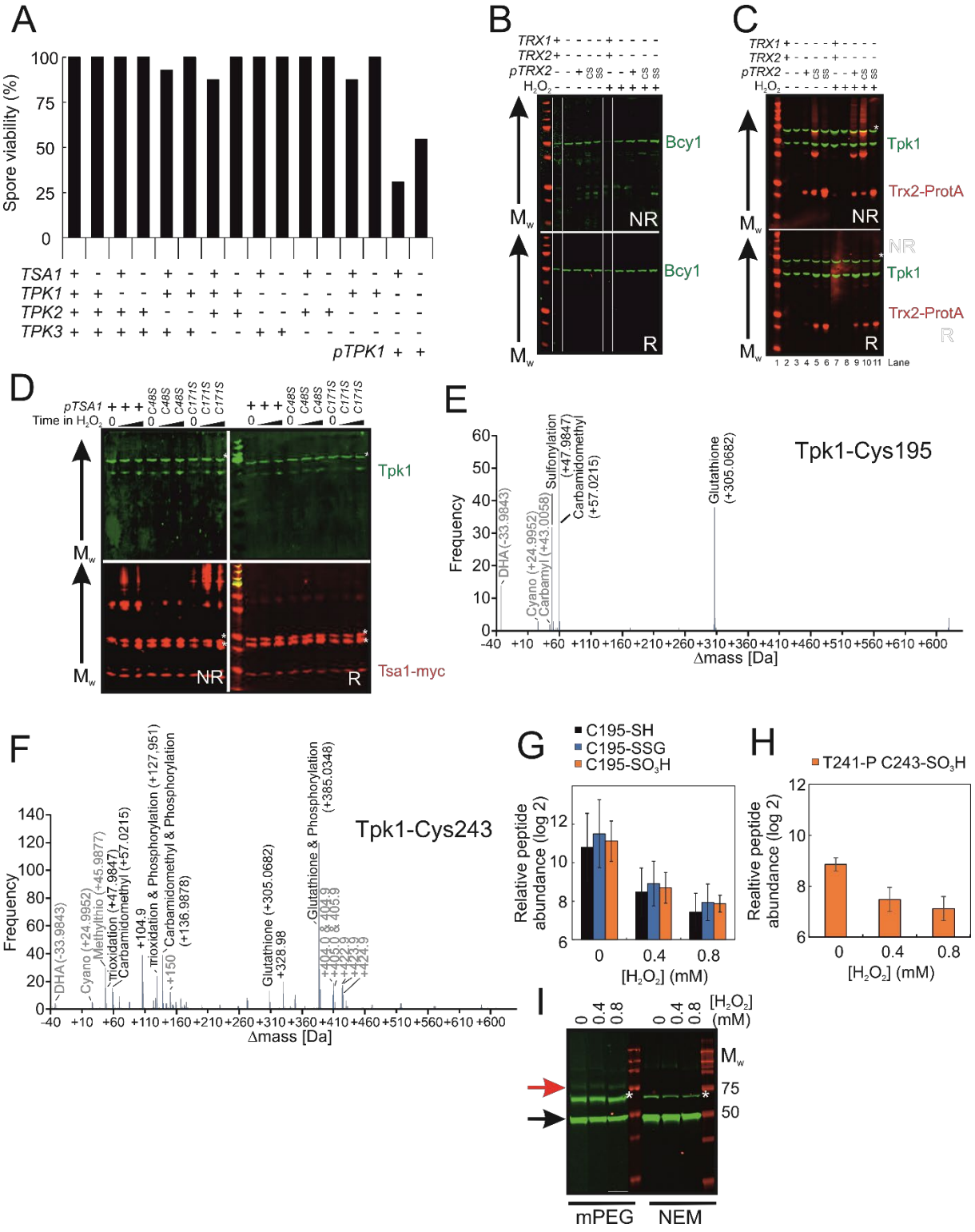

Figure S3. Related to Figure 5. Tsa1 affects PKA signaling at the level of the PKA catalytic subunits and in a manner independent on the regulatory subunit Bcy1. **A)** Spore viability in mutants segregating in a *tsa1Δ* x *tpk1Δtpk2Δtpk3Δ* mutant cross. The *tpk1Δtpk2Δtpk3Δ* mutant was kept alive by a Tpk1-expressing plasmid (pRS313-*TPK1*). Spore viability was estimated in 43 tetrads where genotypes could be assigned to all spores (172 spores in total and in 8-15 spores per genotype). **B-C)** Bcy1 (**B**) or Tpk1 (**C**) redox immunoblots of protein extracts isolated from the indicated thioredoxin mutant strains

in the absence of stress (H_2O_2 -) or following the addition of 0.4 mM H_2O_2 for 20 min (H_2O_2 +). NR = non-reducing R = reducing CS = *trx2C34S* SS = *trx2C31SC34S*. **D)** Tpk1 redox immunoblots of protein extracts isolated from the indicated myc-*tsa1* mutant strains in the absence of stress (Time in H_2O_2 = 0) or 10 or 120 min following the addition of 0.4 mM H_2O_2. **E-F)** Mass-shifts in peptides covering the indicated Tpk1 cysteines detected using unbiased open search approaches. Tpk1-Cys195 denotes the F189-K204 peptide whereas Tpk1-Cys243 the Y239-K261 peptide. **G)** PRM-based quantification of the indicated C195 containing Tpk1 peptides (n=3). Error bars indicate SD. **H)** PRM-based quantification of the Thr241 phosphorylated and Cys243 sulfinic acid containing Y239-K261 peptide in Tpk1 (n=3). Error bars indicate SD. **I)** mPEG assay of the oxidation of Tpk1 following the addition of the indicated amount of H_2O_2 for 10 min in a *tpk1Δtpk2Δtpk3Δ* p*tpk1C243A* mutant strain. Cells were treated with H_2O_2, lysed by TCA and reduced cysteines alkylated by NEM. Following reduction by DTT, oxidized cysteines were alkylated by mPEG in half of the extract (mPEG) and to the other half NEM was added as a control (NEM). Arrows indicate Tpk1 (black) and Tpk1-mPEG (red).

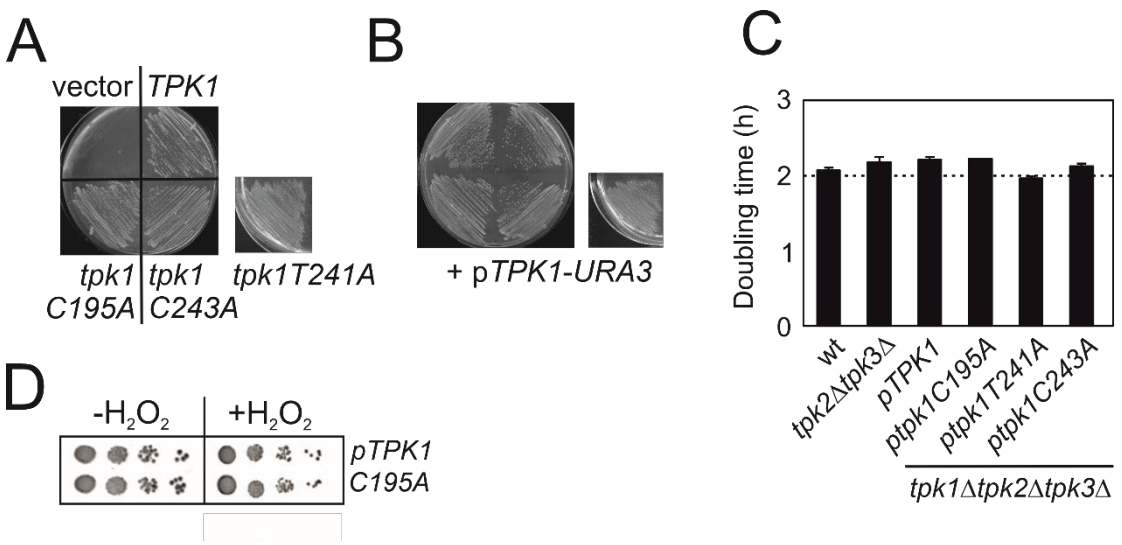

Figure S4. Related to Figure 6. Yeast PKA is redox-regulated by glutathionylation of Tpk1Cys243. **A)** Growth of *tpk1Δtpk2Δtpk3Δ* cells transformed with the vector (vector) or the indicated pRS313-*TPK1* plasmids and pRS316-*TPK1* (p*TPK1-URA3*) on solid synthetic defined (-HIS, 5-FOA) medium to counterselect p*TPK1-URA3*. **B)** Growth of the strains in **A)** on solid synthetic defined selective (-HIS, URA) medium. Cells in **A)** and **B)** were left to grow for 3 days before photographed. **C)** Doubling time of the indicated *tpk*-mutant strains in synthetic defined -HIS medium. **D)** H_2O_2 resistance of *TPK1 tpk2Δ tpk3Δ*□□□□ *tpk1C195A tpk2Δ tpk3Δ*-mutants as indicated.

Detailed materials and methods

Strains and growth conditions

Yeast strains and plasmids are listed in Supplementary Table S1. The strains used in this study are derivatives of BY4741/BY4742. Strains were grown at 30°C in YPD 2% glucose (w/v) or in Yeast Nitrogen Base defined medium containing 2% glucose and complete supplement mixture (CSM) lacking the appropriate amino acids (Formedium) as described previously (Molin et al., 2011). To check the segregation of deletion markers in tetrad dissections YPD medium supplied with the following chemicals was used to check segregation of the dominant markers: *kanMX4* (G418 200 µg/ml), *natMX4* (ClonNAT 100 µg/ml), *hphMX4* (Hygromycin B 300 µg/ml), *bleMX4* (Phleomycin 40 µg/ml). To counterselect the p*TPK1-URA3* plasmid cells were grown in defined glucose CSM – HIS, 5-FOA medium containing YNB, glucose and CSM –URA, HIS; 50 mg/l uracil and 1 g/l 5-fluoroorotic acid.

Strain and plasmid constructions

Strains YMM170 (*ras2*Δ*tsa1*Δ*)* and YMM172 (*pde2*Δ*tsa1*Δ*)* were constructed by crossing strain YMM114 to BY4741 *ras2*Δ*::kanMX4* and BY4741 *pde2*Δ*::kanMX4* [Research Genetics, (Giaever et al., 2002)], respectively, and selecting for Mat alpha, methionine prototrophic, lysine auxotrophic, G418 resistant and nourseothricin resistant progeny. Strains YMM171 and YMM173 were constructed by crossing a BY4741 *pde2*Δ*::hphMX4* {*pde2*Δ*::kanMX4* from the deletion collection [Research Genetics, (Giaever et al., 2002)] marker-switched (Goldstein & McCusker, 1999) to *pde2*Δ*::hphMX4* to strain YMM170 (*ras2*Δ*tsa1*Δ) and selecting for Mat alpha, methionine prototrophic, lysine auxotrophic, G418 resistant, hygromycin resistant and nourseothricin sensitive (YMM171 *ras2*Δ*pde2*Δ) or nourseothricin resistant (YMM173 *ras2*Δ*pde2*Δ*tsa1*Δ) progeny. Strains YMM174 (*msn2*Δ*msn4*Δ), YMM175 (*pde2*Δ) and YMM176 (*pde2*Δ o/e *TSA1*) were constructed by crossing BY4741 *msn2*Δ*msn4*Δ (Caballero et al., 2011) or BY4741 *pde2*Δ*::kanMX4* [Research Genetics, (Giaever et al., 2002)] to strains YMM130 or BY4742 *his3*Δ*1::pRS403-Myc-TSA1*, respectively and selecting for Mat alpha, methionine prototrophic, lysine auxotrophic, histidine auxotrophic, hygromycin- and nourseothricin-resistant progeny (YMM174) or Mat alpha, methionine prototrophic, lysine auxotrophic, G418 resistant and histidine prototrophic progeny (YMM174 and YMM175). Strain YMM177 was constructed by marker-switching (Goldstein & McCusker, 1999) a Mat a *ras1*Δ*::kanMX4* spore, obtained from crossing strain BY4741 *ras1*Δ*::kanMX4* [Research Genetics, (Giaever et al., 2002)] to strain YMM114 and selecting for Mat a, methionine prototrophic, lysine auxotrophic and G418 resistant progeny, to *ras1*Δ*::hphMX4*. Strain YMM178 (*tpk1*Δ*/TPK1 tpk2*Δ*/TPK2 tpk3*Δ*/TPK3*) was constructed by crossing a BY4742 *tpk1*Δ*::kanMX4 tpk2*Δ*::natMX4* strain to a BY4741 *tpk3*Δ*::hphMX4* strain {*tpk3*Δ*::kanMX4* from the deletion collection [Research Genetics, (Giaever et al., 2002)] marker-switched (Goldstein and McCusker, 1999) to *tpk3*Δ*::hphMX4* resulting in a *tpk1Δ/TPK1 tpk2Δ /TPK2 tpk3Δ /TPK3* heterozygous diploid strain. A Mat alpha, nourseothricin- and hygromycin-resistant spore constitutes strain YMM179. The BY4742 *tpk1*Δ*::kanMX4 tpk2*Δ*::natMX4* strain was constructed by introducing *tpk2*Δ*::natMX4* PCR amplified from a BY4742 *tpk2*Δ*::natMX4* strain (Costanzo et al., 2010) into strain BY4741 *tpk1*Δ*::kanMX4* [Research Genetics, (Giaever et al., 2002)] selecting for nourseothricin- and G418-resistance and verifying the deletion by diagnostic PCR. A BY4742 *tpk1*Δ*tpk2*Δ*tpk3*Δ p*TPK1-URA3* haploid strain (YMM180) was constructed by transforming strain YMM177 with plasmid p*TPK1-URA3* and sporulating the strain selecting for a Mat alpha methionine prototrophic, lysine auxotrophic, G418-, nourseothricin-, hygromycin B-resistant and uracil auxotrophic progeny. Strains YMM181-YMM185 were constructed by transforming strain YMM179 with plasmids pRS313 (YMM181), pRS313-*TPK1*

(YMM182), pRS313-*tpk1C243A* (YMM183) and pRS313-*tpk1C243D* (YMM184) and pRS313-*tpk1T241A* (YMM185). Counterselecting p*TPK1-URA3* on 5-FOA medium resulted in strains YMM186 (BY4742 *tpk1*Δ*tpk2*Δ*tpk3*Δ pRS313-*TPK1*), YMM187 (BY4742 *tpk1*Δ*tpk2*Δ*tpk3*Δ pRS313-*tpk1C243A*), YMM188 (BY4742 *tpk1*Δ*tpk2*Δ*tpk3*Δ pRS313-*tpk1C243D*) and yMM189 (BY4742 *tpk1*Δ*tpk2*Δ*tpk3*Δ pRS313-*tpk1T241A*), respectively. Strain YMM190 (*ras2*Δ*trx1*Δ*trx2*Δ) was constructed by crossing strain YMM113 (*ras2*Δ) to strain YMM143 (*trx1*Δ*trx2*Δ) selecting for Mat alpha, methionine prototrophic, lysine auxotrophic, G418-, nourseothricin- and hygromycin B-resistant progeny. Strain YMM191 was constructed by marker-switching strain BY4741 *tsa1*Δ*::kanMX4* [Research Genetics, (Giaever et al., 2002)] into BY4741 *tsa1*Δ*::bleMX4* using a bleMX4 cassette PCR amplified from plasmid pUG66 (Gueldener, Heinisch, Koehler, Voss, & Hegemann, 2002) using primers PR78 and PR79 (Goldstein & McCusker, 1999). Strain yMM192 was constructed by crossing strains yMM179 and yMM191 selecting for a Mat a, nourseothricin+, hygromycin+ and phleomycin+ spore. Strain WR1832 was constructed by first introducing PCR amplified *trp1Δ::kanMX4* DNA (Longtine et al., 1998) into strain YMM179, verification of cassette integration by PCR and loss of the ability to grow without tryptophan supplement and next by *HBH::TRP1* C-terminal tagging of *TPK1* and PCR based verification as described (Tagwerker et al., 2006). Strains yCP101-yCP104 were constructed by crossing Mat a *his3Δ1::pRS403* or *his3Δ1::pRS403-myc-TSA1* spores, obtained in crosses generating strains yMM175 above, either to strain yMM182 or to strain yMM186 also carrying plasmid *pRS316-tpk1C243A*. Methionine prototrophic, lysine auxotrophic, histidine prototrophic, 5-FOA-sensitive, G418+, nourseothricin+ and hygromycin B+ progeny obtained in these crosses constitute strains yCP101-yCP104 listed in Table S1. Strains yCP105 and yCP106 were constructed by crossing strains yMM186 (p*TPK1*) or yMM189 (p*tpk1T241A*), respectively, to strain yMM192 selecting for Mat alpha, Met+, Lys-, G418+, Nat+, Hyg+, Phleomycin+, His+ progeny. Strain yCP107 was constructed by crossing strain WR1832 to yMM192 and selecting for Mat alpha, Met+, Lys-, G418+, Nat+, Hyg+, Phleomycin+, Trp+ progeny.

Plasmids pRS313-*tpk1C243A*, pRS313-*tpk1C243D*, pRS313-*tpk1T241A* and pRS316-*tpk1C243A*, were constructed by site directed mutagenesis of the pRS313-*TPK1* or pRS316-*TPK1* plasmids (Eurofins Genomics). Plasmids pRS315-*trx1C34S*-ProtA and pRS315-*trx2C31SC34S*-ProtA were constructed by site-directed mutagenesis of plasmid pRS315-*TRX2*-ProtA (GenScript). The correct sequence of all plasmids constructed was verified by sequencing.

Global H_2O_2 scavenging in the medium

Medium peroxide determinations were performed using a ferrithiocyanate spectrophotometric assay (Molin et al., 2007). After bolus addition of H_2O_2, 100 µL sample aliquots were withdrawn and cultures were arrested by the addition of 1 ml ice-cold 10% TCA. After pelleting cells 180 mM KSCN and 1.4 mM $Fe(NH_4)_2(SO_4)_2$ final concentrations were added to the supernatants. Absorbance at 480 nm was subsequently determined and compared to equally TCA-treated H_2O_2 standards diluted in medium.

Isolation of old cells

Old cells were obtained as previously described by sorting biotin-labeled mother cells using the MagnaBind streptavidin system (Sinclair and Guarente, 1997). Briefly, mid-exponential phase cells were labeled with EZ-Link Sulfo-NHS-LC Biotin and grown overnight in minimal media (CSM-His). The cells were incubated with streptavidin-conjugated magnetic beads for 2 h and then sorted magnetically with the unlabeled cells being washed away. Sorted cells were then grown overnight and

the streptavidin labeling procedure was repeated before sorting one last time. After sorting the cells were incubated for 1 h in CSM-His media at 30 ◦C for recovery before microscopy.

Measurements of cytoplasmic H_2O_2 using HyPer3

Fluorescence of the ratiometric probe HyPer-3 (Bilan et al., 2013) was acquired using an Olympus IX81 motorized microscope with a PlanApoN 60x/1.42 Oil objective and a 12-bit Hamamatsu camera. Shifts in the fluorescence intensities were acquired with excitation around 500 nm (485/20 nm) and 420 nm (427/10 nm filter) and an emission filter around 520 nm (Fura 2 filter). For bolus addition of H_2O_2, cells in midexponential phase were incubated with 0.2 mM H_2O_2 for 10 min and immediately imaged.

Image Analysis

Image and signal analysis was performed using the MATLAB toolbox 2016b. Cell segmentation is performed with the CellX algorithm using the bright-field channel. The fluorescent intensity data was obtained from fluorescent images and data is presented as the median 500 nm fluorescent signal normalized to the median fluorescent 420 nm signal by dividing the latter with the former.

Lifespan Analyses

Lifespan analyses were performed as previously described by counting the number of daughters produced in a cohort of mother cells (Erjavec et al., 2007).

Spot tests

H_2O_2 resistance was tested with mid-exponential-phase (A_{600}=0.5, 5 × 10^6 cells/ml) cells that were diluted (x5, x50, x500, x5000, x50000) and spotted onto SD media containing 0 to 1 mM H_2O_2 or YPD media containing 0 to 2 mM. The plates were incubated at 30 ◦C for 3 days. For glycogen accumulation, plates incubated for 2 days at 30 ◦C were exposed to iodine-bead fumes for 2.5 min and scanned immediately.

Quantitative Real-Time PCR Analysis

Cell cultures were harvested in mid-exponential phase and resuspended in 1 ml Trizol Reagent (Invitrogen) and homogenized with silica beads by Fast prep (6.5 m/s, 30 sec, interval 2.5min, 4 ◦C). RNA was extracted using phenol chloroform extraction and precipitated with sodium acetate/ethanol. The pellet was treated with DNase for 30min followed by heat-inactivation of the enzyme. The RNA was purified with Invitrogen PureLink RNA Mini Kit columns and converted to cDNA following the QIAGEN QuantiTect Reverse Transcription Kit. Q-PCR was performed with 50ng cDNA by using BioRad iQ SYBR Green Supermix and quantified with the BioRad iCycler, iQ5. Relative levels of mRNA were calculated by using cycle times of *ACT1* as a reference gene.

2D-PAGE

Protein synthesis rates of the indicated proteins were determined in ^{35}S-Methionine labelled protein extracts separated by two-dimensional polyacrylamide gel electrophoresis as described (Maillet et al., 1996; Molin et al., 2011). Tsa1 sulfinylation was determined by comparing levels of sulfinylated Tsa1 (Tsa1-SOOH) to non-sulfinylated Tsa1 on silver-stained 2D gels as described (Molin et al., 2011).

Measurement of Ras2-GTP *in vivo*

Ras2-GTP level were measured as a ratio between Ras2-GTP and total Ras2 as described previously (Colombo & Martegani, 2014; Peeters et al., 2017). Mid-exponential phase yeast cells were harvested and lysed with glass- beads in Fast-prep (6.0 m/s, 20sec, interval 2.5 min) in lysis buffer [50 mM Tris-HCl, 200 mM NaCl, 2.5 mM $MgCl_2$, 10% glycerol, 1% Triton X100, cOmplete Protease inhibitor EDTA-free]. The supernatant with 1.5mg of total protein was incubated with a bed volume 50 µL of glutathione S-transferase (GST)-RBD fusion protein pre-bound to glutathione-Sepharose for 1 h at 4 ◦C and washed three times with lysis buffer by centrifugation. For elution the beads were boiled for 5 min at 98 ◦C in SDS-sample buffer (6% SDS, 62.5 mM Tris-HCl pH 8.7, 30% Glycerol, 0.75% β-mercaptoethanol). Through western blotting, Ras2-GTP and total Ras2 proteins were detected with anti-Ras2 antibodies. Determination of ratios between Ras2-GTP and total Ras2 was performed by ImageJ.

cAMP measurement

cAMP measurements were performed as previously described (Caballero et al., 2011; Parts et al., 2011). 2×10^8 cells grown to midexponential phase were pelleted, washed, and resuspended in 1 ml cold milliQ water. Metabolites were extracted by adding 1.2 ml TCA (0.5 M) and occasional vigourous vortexing while samples were kept on ice for 15 min. TCA was removed by ether extraction. cAMP levels were determined by the LANCE cAMP 384 kit in 40 µL total reactions and by comparing to the standards supplied. The values for cAMP were normalized to the wild type level.

Spore viability

The viability of spores segregating in the sporulation and dissection of a heterozygous diploid *ras1*Δ*::hphMX4/RAS1 ras2*Δ*::kanMX4/RAS2 tsa1*Δ*::natMX4/TSA1* strain obtained by crossing strain YMM176 (*ras1*Δ*::hphMX4*) to strain YMM170 (BY4742 *ras2*Δ*::kanMX4 tsa1*Δ*::natMX4*) was analyzed after 4 days of incubation at 30°C in 32 tetrads where 1) all markers analyzed (*hphMX4, kanMX4, natMX4, MET15, LYS2*) segregated 2:2, 2) the exact genotypes of all spores were possible to deduce from this information and 3) the genotypes of dead spores were assigned based on markers present in the other spores dissected from the same tetrads. Similarly, spore viability of spores segregating in a heterozygous diploid *tpk1*Δ*::kanMX4/TPK1 tpk2*Δ*::natMX4/TPK2 tpk3*Δ*::hphMX4/TPK3 tsa1*Δ*::bleMX4/TSA1*, obtained by crossing strain YMM191 (BY4741 *tsa1*Δ*::bleMX4*) to strain YMM186 (BY4742 *tpk1*Δ*::kanMX4 tpk2*Δ*::natMX4 tpk3*Δ*::hphMX4* expressing pRS313-*TPK1*), was analyzed in 43 tetrads where all chromosomal markers analyzed (*kanMX4, natMX4, hphMX4, bleMX4, MET15, LYS2*) segregated 2:2. The ability to grow in the absence of histidine supplementation (-HIS) was taken as an indication that the pRS313-*TPK1* plasmid was present.

Immunoblot analysis

Immunoblot analysis of selected proteins was performed as described previously (Biteau, Labarre, & Toledano, 2003; Molin et al., 2011). Prior to separation on 12% Bis-Tris NuPAGE gels using an XCell SureLock MiniCell (Invitrogen) in NuPAGE MOPS running buffer as recommended by the supplier protein extracts were heated in Laemlii buffer (pH 8.7) either in the presence of β-mercaptoethanol (5%, reducing) or not (non-reducing) as indicated. Transfer to Immobilon-FL PVDF membranes was done using an XCell II Blot Module kit. Membranes were analyzed by the Odyssey infrared imaging system (LI-COR biosciences) as recommended by the suppliers.

Glutathionylation of Tpk1 was assayed using anti-glutathione immunoblot on Tpk1-HB immunoprecipitated by Ni^{2+}-Sepharose beads following a simplified protocol similar to that used

during MS sample preparation (see below). We verified that the anti-glutathione immunoblot signal in Tpk1 completely disappeared upon extract reduction by β-mercaptoethanol.

Growth conditions for MS analysis

Cells were grown at 30°C in yeast extract/peptone (YP) medium, containing 2% glucose as carbon source. Three independent experimental replicates were performed for each experimental condition. For each replicate, we inoculated 750ml YPD cultures, which were incubated (with shaking) overnight until OD600 = 1. Oxidative stress was induced by adding 0.4 mM or 0.8 mM (final concentration) H_2O_2 for 10 minutes.

Mass spectrometric sample preparation

HB (poly histidine, biotinylation signal) tandem affinity purifications were performed as described elsewhere (Reiter et al., 2012). Cells were harvested by filtration and immediately deep-frozen in liquid N_2. Cells were grinded using a SPEX Freezer Mill 6870 (SPEXSamplePrep, Metuchen, NJ, USA) with the following settings: 7 cycles: 3 min breakage (15 CPS), 3 min cooling, resuspended in buffer 1 (6 M guanidine HCl, 50 mM Tris pH8.0, 5 mM NaF, 1 mM PMSF, 0.1% Tween, cOmplete Protease inhibitor cocktail, pH 8) and cleared of debris by centrifugation 13.500 x g, 15 min, 4°C. Cleared extracts were incubated (4 hours, room temperature) with Ni^{2+}-Sepharose beads, washed with urea buffer (8M urea, 50mM sodium phosphate buffer pH8.0, 300mM NaCl, 0.1% Tween20) and urea buffer pH 6.3. Proteins were eluted in urea buffer pH 4.3 containing 10mM EDTA, incubated overnight with streptavidin-agarose beads, washed using urea wash buffer containing 1% SDS and urea wash buffer without SDS. Beads were washed five times with 50 mM ammonium bicarbonate (ABC). Cys-residues were alkylated with IAA (25% w/w of the estimated amount of protein). Excess IAA was washed out by ABC. Proteins were digested with 300 ng trypsin at 37°C overnight. Digestion was stopped with trifluoroacetic acid (0.5% final concentration) and the peptides were desalted using C18 Stagetips (Rappsilber, Mann, & Ishihama, 2007). 50 fmol of the Peptide Retention Time Calibration Mixture was spiked in each sample for quality control.

Mass spectrometry analysis of Tpk1

Peptides were separated on an Ultimate 3000 RSLC nano-flow chromatography system (Thermo-Fisher), using a pre-column (Acclaim PepMap C_{18}, 2 cm × 0.1 mm, 5 µm, Thermo-Fisher), and a C_{18} analytical column (Acclaim PepMap C18, 50 cm × 0.75 mm, 2 µm, Thermo-Fisher). A segmented linear gradient from 2% to 35% solvent B (solvent B: 80% acetonitrile, 0.1% formic acid; solvent A: 0.1% formic acid) was applied at a flow rate of 230 nL/min over 120 min. A Proxeon nanospray flex ion source (Thermo Fisher) using coated emitter tips (New Objective) was used for ionization. The capillary temperature was set to 200°C. Peptides were analyzed on an Orbitrap Fusion Lumos Tribrid mass spectrometer (Thermo Fisher). The mass spectrometer was operated in data-dependent mode, survey scans were obtained in a mass range of 380-1500 m/z with lock mass activated, at a resolution of 120,000 at 200 m/z and an automatic gain control (AGC) target value of 4E5. The maximum cycle time was set to 2.5 s and the most abundant precursors were selected for fragmentation by high-energy collision at 30% collision energy. Fragmented precursors were excluded from further fragmentation for 30s (with +/- 5 ppm accuracy) and peptides with charge +1 or > +6 were excluded from MS/MS analysis. The most abundant Tpk1 Cys containing peptide forms have been added to an inclusion list as specified in the raw files. MS proteomics data have been deposited to the ProteomeXchange Consortium through the Proteomics Identifications database (PRIDE) partner repository (Vizcaino et al., 2016) with the data set identifiers PXD012617.

Closed database search

Peptide identification and label free quantification (LFQ) were performed using MaxQuant (version 1.6.0.16) with default parameters. *Saccharomyces cerevisiae* reference proteome database (UniProt, version January 2017) in combination with a common laboratory contaminants database (MQ) was used for peptide spectrum matching. N-terminal acetylation, deamidation of asparagine and glutamine, oxidation of methionine, tri-oxidation and glutathionylation of cysteine and phosphorylation of serine, threonine and tyrosine were set as variable protein modification. Carbamidomethylation of cysteine was set as fixed. A maximum of 5 variable modifications per peptide was allowed. Leucine and isoleucine were treated as indistinguishable. Enzyme specificity was set to "Trypsin/P". A maximum of 2 missed cleavages per peptide was allowed. 'Requantify' and "Match between runs" was activated. MaxLFQ (implemented in the MaxQuant package) was used for MS1-based label free quantification and normalization of protein groups.

Open search analysis of selected peptides

To screen for protein modifications in an unbiased manner we initially performed an open search using MSFragger in FragPipe (Kong, Leprevost, Avtonomov, Mellacheruvu, & Nesvizhskii, 2017). The default open search parameters were used, with trypsin specificity, +/- 500 Da windows and oxidation of methionine and carbamidomethylation of cysteine as variable modifications. The observed mass shifts were inspected and filtered for the most abundant and relevant modifications occurring in Tpk1.

Targeted mass-spectrometry

Parallel-Reaction-Monitoring (PRM) assays were generated based on the peptide information obtained by MaxQuant. We selected Tpk1 and Tsa1 peptides for targeted relative LFQ as specified in Expanded View tables XY, datasheets 4 to 6.Peptides were separated using a 120 min gradient (HPLC setup as described above). PRM data acquisition was performed using a scheduled method with 20 min windows for each target based on the retention time determined in the shotgun-approach. Raw data were obtained on an Orbitrap Q Exactive HF-X (Thermo Fisher Scientific) mass spectrometer applying the following settings: survey scan with 60k resolution, AGC 1E6, 60 ms IT, over a range of 400 to 1400 m/z, PRM scan with 30 k resolution, AGC 1E5, 200 ms IT, isolation window of 1.0 m/z with 0.3 m/z offset, and NCE of 27%.

Wash runs were checked for potential peptide carry-over in between samples using same HPLC and MS methods. Data analysis, manual validation of all transitions (based on retention time, relative ion intensities, and mass accuracy), and relative quantification was performed in Skyline. Up to six characteristic transitions were selected for each peptide and their peak areas were summed for peptide quantification (total peak area). MS1 signals of PRTC standards were used as global standards for normalization in Skyline to account for fluctuations in instrument performance. The mean of the log2 Tpk1 non-modified peptide intensities was used to normalize Tpk1 modified peptides and Tsa1 peptides to account for differences in Tpk1 levels. Tsa1 peptide intensities (anti-log) were summed up to obtain values for relative protein abundance.

mPEG assay

To assay oxidation of the Tpk1 protein the immunoblot procedure was adapted to the mPEG-switch assay (Burgoyne et al., 2013) in the following way. Following TCA lysis, protein extraction and acetone wash dried protein was re-dissolved in buffer A (1% SDS, 10 mM EDTA, 0.1 M Tris pH 8.8),

containing 50 mM NEM to alkylate reduced cysteines. Proteins were next precipitated with TCA, washed with acetone, protein pellets dried and re-dissolved in buffer A containing 5 mM DTT to reduce oxidized cysteines. Following an additional round of TCA precipitation, acetone wash and lyophilization the dry protein pellets were subsequently dissolved in buffer B (1% SDS, 10 mM EDTA, 0.1 M Tris pH 8.0) containing either 1) 2 mM methoxypolyethylene glycol maleimide (mPEG) or 2) 50 mM NEM. Extracts were next subjected to SDS-PAGE (10% Criterion TGX Gels) gel electrophoresis under reducing conditions using a Criterion cell. Proteins were blotted to membranes using a Criterion Blotter and analyzed as above.

Homology modeling

A model of the yeast PKA tetramer structure was obtained by homology modeling. The protein sequences of yeast Tpk1 (catalytic subunit of PKA) and Bcy1 (regulatory subunit of PKA) were obtained from Genbank (ID: 1023942850 and ID: 1023943330, respectively). The crystal structure of mouse PKA (PDBID: 3TNP) was used as the template for the homology calculations. The catalytic and regulatory subunits of yeast PKA and mouse PKA shares 48% and 42% sequence similarity, respectively. The homology model was built using StructurePrediction panel (Jacobson, Friesner, Xiang, & Honig, 2002) in Schrödinger Suite (Schrödinger, LLC, New York, NY). The ClustralW method was used to align the target and template sequences in Prime, the energy-based was selected for model building method, and homo-multimer was selected for multi-template model type.

Covalent docking

Covalent docking was carried out to obtain a model for glutathionylated Tpk1. The Tpk1 crystal structure [PDB ID: 1FOT, (Mashhoon, Carmel, Pflugrath, & Kuret, 2001)] were prepared using the Protein Preparation utility in Schrodinger to assign the correct protonation state and fix the missing side chains and loops. The glutathione was built by 3D builder and prepared by LigPre utility in Schrodinger. The Covalent-Dock panel (Zhu et al., 2014) in Schrodinger was used to predict the pose of the glutathione attaching to Cys243. The reaction type was set to be disulfide formation, the docking mode was set to be thorough pose prediction, the other parameters were all set to be default. At the final step, Prime Energy was used to rank the poses of the ligand. Covalent docking was performed on dephosphorylated Tpk1 structure.

Molecular dynamics simulations

Molecular dynamics simulations were carried out to study structural changes of Tpk1 upon phosphorylation and glutathionylation. MD simulations non-modified Tpk1, Cys243 glutathionylation Tpk1, Thr241 phosphorylation Tpk1, Cys243 glutathionylation and Tpk1 phosphorylation co-existed Tpk1 were carried out. The GROMACS software (Abraham et al., 2015) was used for the MD simulations and the Amber 99 (Ponder & Case, 2003) force field was selected to assign the parameters for different amino acid residues. The glutathionylation and phosphorylation parameters was generated from Ambertools, and incorporated into the GROMACS software.

The systems were solvated with a buffer distance of 10.0 Å TIP3P water in periodic boxes, and then 0.1 mol/L of Na^+ and Cl^- ions were added to adjust the systems to electroneutrality condition. Then 200 steps of the steepest descent energy minimization was carried out to remove close contacts in the obtained systems. A 2ns position-restrained simulation with a constant pressure ensemble (NPT) was performed to make sure the water molecules would reach more favorable positions. The parameters for position-restrained simulation are set to be: a time step = 1 fs, temperature = 298 K, and coupling pressure = 1 bar, Coulomb cutoff = 10 Å, Lennard-Jones cutoff = 10 Å, particle-mesh Ewald

summation (Darden, York, & Pedersen, 1993; Essmann et al., 1995) was used for longrange electrostics. The temperature and pressure was controlled by Berendsen coupling algorithm (Berendsen, Postma, Vangunsteren, Dinola, & Haak, 1984), with the time constants of 0.1 ps for temperature and 1.0 ps for pressure coupling. All bond lengths was contrained by the LINCS algorithm (Hess, Bekker, Berendsen, & Fraaije, 1997). Following the position-restrained simulation, 100 ns production simulations with NPT ensemble were performed on each system for further study the protein conformational changes. In this step, the Nose– Hoover thermostat (Hoover, 1985), with a time constant 0.1 ps, was used to control the temperature and the Parrinello–Rahman barostat (Parrinello & Rahman, 1981), with a time constant 1.0 ps, was used to control the pressure. The other parameters were the same as those in the position-restrained simulations.

Quantification and statistical analysis

All experiments were repeated at least three times (biological replicates) to ensure reproducibility. Details on the number of replicates and statistical analyses performed are available below.

Figure 1. A) Lifespans were tested for statistical significance by the Mann-Whitney U test (www.socscistatistics.com/tests/mannwhitney/Default2.aspx). Lifespans of the wt (n=168) vs the *tsa1Δ* mutant (n=293), wt vs *tsa1C48S* (n=70), wt vs *tsa1C171S* (n=120), *tsa1ΔYF* (n=255) vs *tsa1ΔYFC171S* (n=70) are all different at p<0.00001. The lifespan of the *tsa1ΔYF* mutant is different from the wt at p<0.00854 whereas no significant difference was seen between the *tsa1Δ* vs *tsa1C48S* (p=0.1074), *tsa1C48S* vs *tsa1C171S* (p=0.3125), *tsa1ΔYFC171S* vs *tsa1C171S* (p=0.23014). **B)** The scavenging rates of the wt and the *tsa1Δ* mutant following the addition of 0.4 mM are not significant in a two-tailed t-test assuming equal variance (p=0.684). **C)** Fluorescence ratios 500/420 nm of the HyPer3 expressing strains are significantly different between the wt young (n=231) vs old (n=319) ($p=2.42 \times 10^{-13}$) and wt young vs wt young $+H_2O_2$ (n=202) ($p=5.27 \times 10^{-76}$) but not when comparing wt old vs *tsa1Δ* old (n=236)(p=0.101). **D)** Fluorescence ratios 500/420 nm of the HyPer3 expressing strains are neither significantly different between the wt young (n=404) vs the o/e *TSA1* young (n=579, p=0.069) nor the wt old (n=190) vs o/e *TSA1* old (n=204, p=0.755).

Figure 2. B) Lifespans of the wt (n=157) vs the *tsa1Δ* (n=293) and the *tsa1Δ* vs *ras2Δtsa1Δ* (n=283) are significantly different at p<0.00001. The lifespan of the *ras2Δ* (n=138) is not significantly different from the *ras2Δtsa1Δ* (p=0.276). **D)** H_2O_2 resistance is significantly different between wt and *ras2Δ* strains (p=0.013), wt and *tsa1Δ* (p=0.0049) and *tsa1Δ* and *ras2Δ tsa1Δ* (p=0.010). **E)** Lifespans of the wt (n=157) vs the *pde2Δ* (n=120), the *ras2Δtsa1Δ* vs *ras2Δpde2Δtsa1Δ* (n=164) and the *tsa1Δ* (n=293) vs *pde2Δtsa1Δ* (n=242) are significantly different at p<0.00001. Lifespans of the *ras2Δpde2Δ* (n=124) vs *pde2Δ* are significantly different (p=0.00068) whereas the lifespans of *pde2Δ* vs *pde2Δtsa1Δ* are not significantly different (p=0.757). **F)** H_2O_2 resistance is significantly different between wt vector and mc-*IRA2* strains (p=0.045), *tsa1Δ* vector and mc-*IRA2* strains (p=0.0064), *tsa1Δ* mc-*IRA2* and *pde2Δtsa1Δ* mc-*IRA2* strains (p=0.0065) but not *pde2Δ* vector and mc-*IRA2* strains (p=0.40).

Figure 3. A) Doubling times of wt and *ras2Δ* strains are significantly different at p=0.047 whereas the difference between the *tsa1Δ* and the *ras2Δtsa1Δ* is not statistically significant using a two-sided t-test assuming equal variance (p=0.77). **C)** Doubling times of control and mc-*IRA2* strains are significantly different for the wt (n=7 each, $p=7.4 \times 10^{-6}$), the *tsa1ΔYF* (n=3 and 4, respectively, p=0.0032) and *msn2Δmsn4Δ* (n=3 each, p=0.026). In none of the other strains are control and mc-*IRA2* different (*tsa1Δ* n=3 each, p=0.87; *tsa1C48S*, n=3 each, p=0.71; *tsa1C171S*, n=4 each, p=0.11; *tsa1ΔYFC171S*, n=4 each, p=0.77; *pde2Δ*, n=3 each, p=0.66; *trx1Δtrx2Δ*, n=4 each, p=0.90. **D**) Relative *HSP12* levels were

significantly different between wt control and mc-*IRA2* strains (n=15 and 9, respectively, p=1.0 x 10^{-14}), between wt mc-*IRA2* and *tsa1Δ* mc-*IRA2* strains (n=9 and 8, respectively, p=1.9 x 10^{-6}), between wt mc-*IRA2* and *tsa1C171S* mc-*IRA2* strains (n=9 and 4, respectively, p=0.026), between wt mc-*IRA2* and *tsa1ΔYFC171S* mc-*IRA2* strains (n=9 and 6, respectively, p=0.00083) and between wt mc-*IRA2* and *pde2Δ* mc-*IRA2* strains (n=9 and 6, respectively, p=4.8 x 10^{-8}). No significant difference was seen between wt mc-*IRA2* and *tsa1ΔYF* mc-*IRA2* strains (n=9 and 3, respectively, p=0.53). Relative *CTT1* levels were significantly different between wt control and mc-*IRA2* strains (n=24 and 21, respectively, p=3.4 x 10^{-13}), between wt mc-*IRA2* and *tsa1Δ* mc-*IRA2* strains (n=21 and 6, respectively, p=0.0073), between wt mc-*IRA2* and *tsa1C171S* mc-*IRA2* strains (n=9 and 4, respectively, p=0.026), between wt mc-*IRA2* and *tsa1ΔYF* mc-*IRA2* strains (n=21 and 3, respectively, p=0.027), between wt mc-*IRA2* and *tsa1ΔYFC171S* mc-*IRA2* strains (n=21 and 6, respectively, p= p=4.9 x 10^{-5}) and between wt mc-*IRA2* and *pde2Δ* mc-*IRA2* strains (n=21 and 6, respectively, p=3.5 x 10^{-7}). **F)** Doubling times of control and mc-*IRA2* strains are significantly different for the wt control (n=3 each, p=0.00042), the wt o/e *PDE2* (n=3 each, p=0.00091) and for the *tsa1Δ* mc-*PDE2* strain (n=3, p=0.0058) but not for the *tsa1Δ* control strain (n=3 each, p=0.20).

Figure 4. A) Lifespans of wt control and o/e *TSA1* strains (Hanzen et al., 2016) are significantly different using the Mann Whitney U test (n=377 and 439 cells, p= 1.0x10^{-25}. Lifespans of *pde2Δ* control and *pde2Δ* o/e *TSA1* strains are not significantly different (n=81 and 84, respectively, p=0.58). **C)** Hsp12 levels are significantly different between control and o/e *TSA1* strains (n=3, p=0.033) whereas Act1 levels are not (n=3, p=0.69). **D)** H_2O_2 resistance is significantly different between wt control and o/e *TSA1* strains (p=0.0085), between wt o/e *TSA1* and *pde2Δ* o/e *TSA1* strains (p=0.0082) but not between *pde2Δ* control and o/e *TSA1* strains (p=0.56).

Figure 5. A). Relative Ras2-GTP/total Ras values in the control and mc-*IRA2* are significantly different in a two tailed t-test with unequal variance for the wt (n=3, p=0.0041). Values for the *pde2Δ* control vs mc-*IRA2* (n=3, p=0.015) and the *tsa1Δ* control vs mc-*IRA2* (n=3, p=0.030) are significantly different in a two-tailed t-test with equal variance. **B)** cAMP levels are significantly different only between wt and *pde2Δ* strains (n=4 each, wt yEP24 vs pde2 yEP24, p=0.0050 and wt pKF56 vs pde2 pKF56, p=1.4 x 10^{-5}). No significant differences were seen between wt and *tsa1Δ* strains (n=4 each, wt yEP24 vs *tsa1Δ* yEP24, p=0.86 and wt pKF56 vs *tsa1Δ* pKF56 p=0.47) or between the wt yEP24 and wt pKF56 (p=0.13). **E**) The abundances of all the three T241-phosphorylated peptides decreased significantly upon adding either 0.4 mM or 0.8 mM H2O2 (for the C243-SH peptide p=0.05 and 0.037 respectively, for the C243-SSG peptide p=0.015 and 0.025 respectively whereas for the C243-SO_3H peptide p=0.011 and 0.0049, respectively. The quantity of the C243-SH T241 non-modified peptide did not change significantly upon the addition of 0.4 and 0.8 mM H_2O_2 (p=0.20 and 0.54, respectively) whereas the C243-SSG T241 non-modified peptide increased significantly following 0.4 mM (p=0.038) but not at 0.8 mM (p=0.17).

Figure 6. G) H_2O_2 resistance is significantly different between wt pRS313 vector control and *tpk2Δtpk3Δ* pRS313 vector control strains (p=0.030), *tpk1Δtpk2Δtpk3Δ pTPK1* and *ptpk1C243A*strains (p=0.030), *tpk1Δtpk2Δtpk3Δ pTPK1* and *ptpk1T241A* strains (p=0.0020) but not *tpk2Δtpk3Δ* pRS313 and *tpk1Δtpk2Δtpk3Δ pTPK1* strains (p=1.00). **I)** Tpk1-S-SG levels are significantly different between wt with and without H_2O_2 (p=0.012), but not between wt and *tsa1Δ* without H_2O_2 (p=0.453) or in the *tsa1Δ* with and without H_2O_2 (p=0.264). **J)** H_2O_2 resistance is significantly different between control *pTPK1* and *ptpk1C243A* strains (p=0.043), control *pTPK1* and *pTSA1 pTPK1* strains (p=0.0072), *pTSA1 pTPK1* and *ptpk1C243A* strains (p=0.0014) but not between control *ptpk1C243A* and *pTSA1*

ptpk1C243A strains (p=0.064). **K)** H_2O_2 resistance is significantly different between *TSA1 pTPK1* and *ptpk1T241A* strains (p=0.022), *TSA1 pTPK1* and *tsa1Δ pTPK1* strains (p=0.031), *tsa1Δ pTPK1* and *ptpk1T241A* strains (p=0.013) but not between *TSA1* and *tsa1Δ ptpk1T241A* strains (p=0.090).

Supplementary Table S1. Key resources table

REAGENT or RESOURCE	SOURCE	IDENTIFIER
Antibodies		
Mouse monoclonal anti-Tpk1	Santa Cruz Biotechnology	Sc-374592, RRID: AB_10990730
Goat polyclonal anti-Bcy1	Santa Cruz Biotechnology	Sc-6734, RRID: AB_671758
Rabbit IgG (anti-ProtA)	Sigma Aldrich	I5006, RRID: AB_1163659
Goat polyclonal anti-Ras2	Santa Cruz Biotechnology	Sc-6759, RRID: AB_672465
Mouse monoclonal anti-Glutathione [D8]	Abcam	ab19534, RRID: AB_880243
Bacterial and Virus Strains		
E. coli BL21 strain expressing pGEX2T-1-GST-RBD	This study, (Peeters et al., 2017)	
Chemicals, Peptides, and Recombinant Proteins		
G418	Acros Organics	Cat #: 329400050
ClonNAT	Werner Bioagents	Cat #: 5.005.000
Hygromycin B	Formedium	Cat #: HYG5000
Phleomycin	Sigma Aldrich	P9564
5-fluoroorotic acid	Sigma Aldrich	F5013
EZ-Link Sulfo-NHS-LC Biotin	Thermo Fisher	Cat #: 21335
Trichloroacetic acid	Sigma Aldrich	Cat #: T6399
KSCN	Sigma Aldrich	Cat #: P2713
$(NH_4)_2Fe(SO_4)_2 \cdot 6\ H2O$	Sigma Aldrich	Cat #: 215406
TRIzol Reagent	Thermo Fisher	Cat #: 15596026
DNase, RNase-free set	Qiagen	Cat #: 79254
cOmplete Mini EDTA-free protease inhibitor	Roche Applied Science	Cat #: 11873580001
Glutathione-S-Transferase-Raf1-Binding-Domain (GST-RBD)	This study, (Peeters et al., 2017)	
Glutathione Sepharose beads		

12% Bis-Tris NUPAGE gels	Thermo Fisher	Cat #: NP0349BOX
MOPS running buffer	Thermo Fisher	Cat #: NP0001
Immobilon-FL PVDF membrane	Millipore	Cat #: IPFL00010
Ni^{2+}-Sepharose beads	GE Healthcare	Cat #: 17-5318-06
Trypsin Gold, mass spectrometry grade	Promega	Cat #: V5280
N-ethylmaleimide	Sigma-Aldrich	Cat #: E3876
Methoxypolyethylene glycol maleimide (mPEG)	Sigma Aldrich	Cat #: 63187
10% Criterion TGX Precast Midi Protein Gel	Bio-Rad	Cat #: 5671034
Peptide Retention Time Calibration Mixture	Pierce, Thermo Fisher	Cat #: 88320
Critical Commercial Assays		
PureLink RNA Mini kit	Thermo-Fisher	Cat #: 12183025
QuantiTect Reverse Transcription Kit	Qiagen	Cat #: 205313
iQ SYBR Green Supermix	BioRad	Cat #: 170-8882
LANCE cAMP 384 kit	Perkin Elmer	Cat #: AD0262
Deposited Data		
Tpk1 MS-data	PRIDE	PXD012617
Experimental Models: Organisms/Strains		
BY4742, wt	(Brachmann et al., 1998)	MAT **alpha** *his3Δ1 leu2Δ0 lys2Δ0 ura3Δ0*
YMM145, *tsa1C48S*	(Bodvard et al., 2017)	BY4742 *tsa1C48S*
YMM146, *tsa1C171S*	(Bodvard et al., 2017)	BY4742 *tsa1C171S*
YMM147, *tsa1ΔYF*	(Bodvard et al., 2017)	BY4742 *tsa1(1-184)*
YMM148, *tsa1C171SΔYF*	(Bodvard et al., 2017)	BY4742 *tsa1(1-184)C171S*
YMM114, *tsa1Δ*	(Molin et al., 2011)	BY4742 *tsa1Δ::natMX4*
YMM113, *ras2Δ*	(Molin et al., 2011)	BY4742 *ras2Δ::kanMX4*

YMM170, *ras2Δtsa1Δ*	This study	BY4742 *ras2Δ::kanMX4 tsa1Δ::natMX4*
BY4742, *pde2Δ*	Research Genetics, (Giaever et al., 2002)	BY4742 *pde2Δ::kanMX4*
YMM171, *ras2Δpde2Δ*	This study	BY4742 *ras2Δ::kanMX4 pde2Δ::hphMX4*
YMM172, *pde2Δtsa1Δ*	This study	BY4742 *pde2Δ::kanMX4 tsa1Δ::natMX4*
YMM173, *ras2Δpde2Δtsa1Δ*	This study	BY4742 *ras2Δ::kanMX4 pde2Δ::hphMX4 tsa1Δ::natMX4*
YMM174, *msn2Δmsn4Δ*	This study	BY4742 *msn2Δ::hphMX4 msn4Δ::natMX4*
YMM143, *trx1Δtrx2Δ*	(Bodvard et al., 2017)	BY4742 *trx1Δ::hphMX4 trx2Δ::natMX4*
YMM130, wt control	(Hanzen et al., 2016)	MAT **alpha** *his3Δ1::pRS403, leu2Δ0 lys2Δ0 ura3Δ0*
o/e *TSA1*	(Hanzen et al., 2016)	MAT **alpha** *his3Δ1::pRS403-Myc-TSA1, leu2Δ0 lys2Δ0 ura3Δ0*
YMM175, *pde2Δ control*	This study	MAT **alpha** *his3Δ1::pRS403, leu2Δ0 lys2Δ0 ura3Δ0 pde2Δ::kanMX4*
YMM176, *pde2Δ* o/e *TSA1*	This study	MAT **alpha** *his3Δ1::pRS403-Myc-TSA1, leu2Δ0 lys2Δ0 ura3Δ0 pde2Δ::kanMX4*

YMM177	This study	**MAT a**, *his3Δ1 leu2Δ0 lys2Δ0 ura3Δ0 ras1Δ::hphMX4*
YMM178	This study	BY-2n *met15Δ0/MET15 lys2Δ0/LYS2 tpk1Δ::kanMX4/TPK1 tpk2Δ::natMX4/TPK2 tpk3Δ::hphMX4/TPK3*
YMM179, *tpk2Δtpk3Δ*	This study	BY4742 *tpk2Δ::natMX4 tpk3Δ::hphMX4*
YMM180, *tpk1Δtpk2Δtpk3Δ pTPK1-URA*	This study	BY4742 *tpk1Δ::kanMX4 tpk2Δ::natMX4 tpk3Δ::hphMX4 pRS316-TPK1*
YMM181, *tpk1Δtpk2Δtpk3Δ pTPK1-URA vector control*	This study	BY4742 *tpk1Δ::kanMX4 tpk2Δ::natMX4 tpk3Δ::hphMX4 pRS313 pTPK1-URA3*
YMM182, *tpk1Δtpk2Δtpk3Δ pTPK1-URA pTPK1*	This study	BY4742 *tpk1Δ::kanMX4 tpk2Δ::natMX4 tpk3Δ::hphMX4 pRS313-TPK1 pTPK1-URA3*
YMM183, *tpk1Δtpk2Δtpk3Δ pTPK1-URA3 ptpk1C243A*	This study	BY4742 *tpk1Δ::kanMX4 tpk2Δ::natMX4 tpk3Δ::hphMX4 pRS313-tpk1C243A pTPK1-URA3*
YMM184, *tpk1Δtpk2Δtpk3Δ pTPK1-URA3 ptpk1C243D*	This study	BY4742 *tpk1Δ::kanMX4 tpk2Δ:natMX4 tpk3Δ::hphMX4 pRS313-tpk1C243D pTPK1-URA3*

YMM185, *tpk1Δtpk2Δtpk3Δ pTPK1-URA3 ptpk1T241A*	This study	BY4742 *tpk1Δ::kanMX4 tpk2Δ::natMX4 tpk3Δ::hphMX4 pRS313-tpk1T241A pTPK1-URA3*
YMM186, *tpk1Δtpk2Δtpk3Δ pTPK1*	This study	BY4742 *tpk1Δ::kanMX4 tpk2Δ::natMX4 tpk3Δ::hphMX4 pRS313-TPK1*
YMM187, *tpk1Δtpk2Δtpk3Δ ptpk1C243A*	This study	BY4742 *tpk1Δ::kanMX4 tpk2Δ::natMX4 tpk3Δ::hphMX4 pRS313-tpk1C243A*
YMM188, *tpk1Δtpk2Δtpk3Δ ptpk1C243D*	This study	BY4742 *tpk1Δ::kanMX4 tpk2Δ::natMX4 tpk3Δ::hphMX4 pRS313-tpk1C243D*
YMM189, *tpk1Δtpk2Δtpk3Δ ptpk1T241A*	This study	BY4742 *tpk1Δ::kanMX4 tpk2Δ::natMX4 tpk3Δ::hphMX4 pRS313-tpk1T241A*
YMM190, *ras2Δtrx1Δtrx2Δ*	This study	BY4742 *ras2Δ::kanMX4 trx1Δ::hphMX4 trx2Δ::natMX4*
YMM191	This study	BY4741 *tsa1Δ::bleMX4*
YMM192, *tpk2Δtpk3Δtsa1Δ*	This study	BY4741 *tpk2Δ::natMX4 tpk3Δ::hphMX4 tsa1Δ::bleMX4*
BY4741, wt	(Brachmann et al., 1998)	MAT a *his3Δ1 leu2Δ0 met15Δ0 ura3Δ0*
cdc25-1	Charlie Boone, (Li et al., 2011)	BY4741, *cdc25-1-3'UTR(CDC25)-::kanMX4-3'UTR(SYS1)*

WR1832, *TPK1-HBH tpk2Δtpk3Δ*	This study	BY4742 *TPK1-HBH::TRP1 tpk2Δ::natMX4 tpk3Δ::hphMX4 trp1Δ::kanMX4*
yCP101, *tpk1Δtpk2Δtpk3Δ pTPK1-URA vector control*	This study	MAT **a** *his3Δ1::pRS403, leu2Δ0 lys2Δ0 ura3Δ0 tpk1Δ::kanMX4 tpk2Δ::natMX4 tpk3Δ::hphMX4 pRS316-TPK1*
yCP102, *tpk1Δtpk2Δtpk3Δ ptpk1C243A-URA vector control*	This study	MAT **alpha** *his3Δ1::pRS403, leu2Δ0 lys2Δ0 ura3Δ0 tpk1Δ::kanMX4 tpk2Δ::natMX4 tpk3Δ::hphMX4 pRS316-tpk1C243A*
yCP103, *tpk1Δtpk2Δtpk3Δ pTPK1-URA* o/e *TSA1*	This study	MAT **alpha** *his3Δ1::pRS403-myc-TSA1, leu2Δ0 lys2Δ0 ura3Δ0 tpk1Δ::kanMX4 tpk2Δ::natMX4 tpk3Δ::hphMX4 pRS316-TPK1*
yCP104, *tpk1Δtpk2Δtpk3Δ ptpk1C243A-URA* o/e *TSA1*	This study	MAT **alpha** *his3Δ1::pRS403-myc-TSA1, leu2Δ0 lys2Δ0 ura3Δ0 tpk1Δ::kanMX4 tpk2Δ::natMX4 tpk3Δ::hphMX4* pRS316-*tpk1C243A*
yCP105, *tpk1Δtpk2Δtpk3Δtsa1Δ pTPK1*	This study	BY4742 *tpk1Δ::kanMX4 tpk2Δ::natMX4 tpk3Δ::hphMX4 tsa1Δ::bleMX4 pRS313-TPK1*

yCP106, *tpk1Δtpk2Δtpk3Δtsa1Δ ptpk1T241A*	This study	BY4742 *tpk1Δ::kanMX4 tpk2Δ::natMX4 tpk3Δ::hphMX4 tsa1Δ::bleMX4 pRS313-tpk1T241A*
yCP107, *TPK1-HBH tpk2Δtpk3Δtsa1Δ*	This study	BY4742 *TPK1-HBH::TRP1 tpk2Δ::natMX4 tpk3Δ::hphMX4 trp1Δ::kanMX4 tsa1Δ::bleMX4*
Oligonucleotides		
ACT1F	(Caballero et al., 2011)	For Q-PCR of *ACT1* CTGCCGGTATTG ACCAAACT
ACT1R	(Caballero et al., 2011)	For Q-PCR of *ACT1* CGGTGAATTTCC TTTTGCATT
CTT1F	This study	For Q-PCR of *CTT1* GCTTCTCAATAC TCAAGACCAG
CTT1R	This study	For Q-PCR of *CTT1* GCGGCGTATGTA ATATCACTC
HSP12F	(Caballero et al., 2011)	For Q-PCR of *HSP12* AGGTCGCTGGTA AGGTTC
HSP12R	(Caballero et al., 2011)	For Q-PCR of *HSP12* ATCGTTCAACTT GGACTTGG
Recombinant DNA		
pAMG	(Gorner et al., 1998)	Msn2-GFP expressed under the control of the *ADH1* promoter, centromeric *LEU2* vector
pHyPer3 (pRS416-*GPD-HyPer3*)	This study, (Bilan et al., 2013)	HyPer3 codon-optimized for yeast, in yeast CEN/ARS, pGPD, *URA3* plasmid

pHyPer3C199S (pRS416-*GPD-HyPer3C199S*)	This study, (Bilan et al., 2013)	HyPer3C199S
yCPlac33	(Gietz & Sugino, 1988)	yeast CEN *URA3* vector
pMW1	(Harashima, Anderson, Yates, & Heitman, 2006)	*RAS2* in CEN *URA3* plasmid
yEP24	(Botstein et al., 1979)	yeast 2µ, *URA3* vector
pKF56	(Tanaka et al., 1990)	*IRA2* in yEP24
pRS425	(Christianson, Sikorski, Dante, Shero, & Hieter, 1992)	yeast 2µ, *LEU2* vector
yEP13-*PDE2*	(Hlavata, Aguilaniu, Pichova, & Nystrom, 2003)	*PDE2* in yeast 2µ, *LEU2* plasmid
pRS313	(Sikorski & Hieter, 1989)	yeast CEN/ARS, *HIS3* empty vector
pRS313-*TPK1*	(Voordeckers et al., 2011)	*TPK1* in pRS313
pRS313-*tpk1C243A*	This study	*tpk1C243A* in pRS313
pRS313-*tpk1C243D*	This study	*tpk1C243D* in pRS313
pRS313-*tpk1T241A*	This study	*tpk1T241A* in pRS313
pRS316	(Sikorski & Hieter, 1989)	yeast CEN/ARS, *URA3* empty vector
pRS316- *myc-TSA1*	(Biteau et al., 2003)	Myc-*TSA1* in pRS316
pRS316- *myc-tsa1C48S*	(Molin et al., 2011)	Myc-*tsa1C48S* in pRS316
pRS316- *myc-tsa1C171S*	(Molin et al., 2011)	Myc-*tsa1C171S* in pRS316
pRS315	(Sikorski & Hieter, 1989)	yeast CEN/ARS, *LEU2* empty vector
B561 (pRS315-*RAS2G19V*)	(Bartels, Mitchell, Dong, & Deschenes, 1999)	*RAS2G19V* in pRS315
pRS315-ProtA	This study	ProteinA in pRS315
pRS315-*TRX2-ProteinA*	(Bodvard et al., 2017)	*TRX2-ProtA* in pRS315
pRS315-*trx2C34S-ProteinA*	This study	*trx2C34S-ProtA* in pRS315

pRS315-*trx2C31SC34S-ProteinA*	This study	*trx2C31SC34S-ProtA* in pRS315
yEPlac195	(Gietz & Sugino, 1988)	yeast 2μ, *URA3* vector
pXP1	(Pan & Heitman, 1999)	*TPK1* in yEPlac195
p*TPK1-URA3 (*pRS316-*TPK1)*	Karin Voordeckers	*TPK1* in pRS316
p*tpk1C243A-URA3*	This study	*tpk1C243A* in pRS316
Software and Algorithms		
MATLAB	Mathworks	version 2016b
CellX	(Mayer, Dimopoulos, Rudolf, & Stelling, 2013)	
Scrödinger Suite	Schrödinger LLC	
GROMACS	(Abraham et al., 2015)	
Amber tools	(Salomon-Ferrer, Case, & Walker, 2013)	

Supplementary references

Abraham, M. J., Murtola, T., Schultz, R., Pall, S., Smith, J. C., Hess, B., & Lindahl, E. (2015). GROMACS: High performance molecular simulations through multi-level parallelism from laptops to supercomputers. *SoftwareX, 54*(7), 1932-1940.

Bartels, D. J., Mitchell, D. A., Dong, X., & Deschenes, R. J. (1999). Erf2, a novel gene product that affects the localization and palmitoylation of Ras2 in Saccharomyces cerevisiae. *Mol Cell Biol, 19*(10), 6775-6787.

Berendsen, H. J. C., Postma, J. P. M., Vangunsteren, W. F., Dinola, A., & Haak, J. R. (1984). Molecular-Dynamics with Coupling to an External Bath. *Journal of Chemical Physics, 81*(8), 3684-3690. doi:Doi 10.1063/1.448118

Bilan, D. S., Pase, L., Joosen, L., Gorokhovatsky, A. Y., Ermakova, Y. G., Gadella, T. W. J., . . . Belousov, V. V. (2013). HyPer-3: A Genetically Encoded H2O2 Probe with Improved Performance for Ratiometric and Fluorescence Lifetime Imaging. *ACS chemical biology, 8*(3), 535-542. doi:10.1021/cb300625g

Biteau, B., Labarre, J., & Toledano, M. B. (2003). ATP-dependent reduction of cysteine-sulphinic acid by *S. cerevisiae* sulphiredoxin. *Nature, 425*(6961), 980-984.

Bodvard, K., Peeters, K., Roger, F., Romanov, N., Igbaria, A., Toledano, M. B., . . . Molin, M. (2017). Light-sensing via hydrogen peroxide and a peroxiredoxin. *Nat Commun, 8*, 14791. doi:10.1038/ncomms14791

Botstein, D., Falco, S. C., Stewart, S. E., Brennan, M., Scherer, S., Stinchcomb, D. T., . . . Davis, R. W. (1979). Sterile host yeasts (SHY): a eukaryotic system of biological containment for recombinant DNA experiments. *Gene, 8*(1), 17-24.

Brachmann, C. B., Davies, A., Cost, G. J., Caputo, E., Li, J., Hieter, P., & Boeke, J. D. (1998). Designer deletion strains derived from *Saccharomyces cerevisiae* S288C: a useful set of strains and plasmids for PCR-mediated gene disruption and other applications. *Yeast, 14*(2), 115-132.

Caballero, A., Ugidos, A., Liu, B., Oling, D., Kvint, K., Hao, X., . . . Nystrom, T. (2011). Absence of mitochondrial translation control proteins extends life span by activating sirtuin-dependent silencing. *Molecular cell, 42*(3), 390-400. doi:10.1016/j.molcel.2011.03.021

Christianson, T. W., Sikorski, R. S., Dante, M., Shero, J. H., & Hieter, P. (1992). Multifunctional yeast high-copy-number shuttle vectors. *Gene, 110*(1), 119-122. doi:0378-1119(92)90454-W [pii]

Colombo, S., & Martegani, E. (2014). Methods to study the Ras2 protein activation state and the subcellular localization of Ras-GTP in Saccharomyces cerevisiae. *Methods Mol Biol, 1120*, 391-405. doi:10.1007/978-1-62703-791-4_24

Costanzo, M., Baryshnikova, A., Bellay, J., Kim, Y., Spear, E. D., Sevier, C. S., . . . Boone, C. (2010). The genetic landscape of a cell. *Science, 327*(5964), 425-431. doi:10.1126/science.1180823

Darden, T., York, D., & Pedersen, L. (1993). Particle Mesh Ewald - an N.Log(N) Method for Ewald Sums in Large Systems. *Journal of Chemical Physics, 98*(12), 10089-10092. doi:Doi 10.1063/1.464397

Essmann, U., Perera, L., Berkowitz, M. L., Darden, T., Lee, H., & Pedersen, L. G. (1995). A Smooth Particle Mesh Ewald Method. *Journal of Chemical Physics, 103*(19), 8577-8593. doi:Doi 10.1063/1.470117

Giaever, G., Chu, A. M., Ni, L., Connelly, C., Riles, L., Veronneau, S., . . . Johnston, M. (2002). Functional profiling of the *Saccharomyces cerevisiae* genome. *Nature, 418*(6896), 387-391.

Gietz, R. D., & Sugino, A. (1988). New yeast-*Escherichia coli* shuttle vectors constructed with in vitro mutagenized yeast genes lacking six-base pair restriction sites. *Gene, 74*(2), 527-534.

Goldstein, A. L., & McCusker, J. H. (1999). Three new dominant drug resistance cassettes for gene disruption in *Saccharomyces cerevisiae*. *Yeast, 15*(14), 1541-1553.

Gorner, W., Durchschlag, E., Martinez-Pastor, M. T., Estruch, F., Ammerer, G., Hamilton, B., . . . Schuller, C. (1998). Nuclear localization of the C2H2 zinc finger protein Msn2p is regulated by stress and protein kinase A activity. *Genes Dev, 12*(4), 586-597.

Gueldener, U., Heinisch, J., Koehler, G. J., Voss, D., & Hegemann, J. H. (2002). A second set of loxP marker cassettes for Cre-mediated multiple gene knockouts in budding yeast. *Nucleic Acids Res, 30*(6), e23.

Hanzen, S., Vielfort, K., Yang, J., Roger, F., Andersson, V., Zamarbide-Fores, S., . . . Nystrom, T. (2016). Lifespan Control by Redox-Dependent Recruitment of Chaperones to Misfolded Proteins. *Cell, 166*(1), 140-151. doi:10.1016/j.cell.2016.05.006

Harashima, T., Anderson, S., Yates, J. R., 3rd, & Heitman, J. (2006). The kelch proteins Gpb1 and Gpb2 inhibit Ras activity via association with the yeast RasGAP neurofibromin homologs Ira1 and Ira2. *Molecular cell, 22*(6), 819-830. doi:10.1016/j.molcel.2006.05.011

Hasan, R., Leroy, C., Isnard, A. D., Labarre, J., Boy-Marcotte, E., & Toledano, M. B. (2002). The control of the yeast H_2O_2 response by the Msn2/4 transcription factors. *Mol Microbiol, 45*(1), 233-241.

Hess, B., Bekker, H., Berendsen, H. J. C., & Fraaije, J. G. E. M. (1997). LINCS: A linear constraint solver for molecular simulations. *Journal of Computational Chemistry, 18*(12), 1463-1472. doi:Doi 10.1002/(Sici)1096-987x(199709)18:12<1463::Aid-Jcc4>3.0.Co;2-H

Hlavata, L., Aguilaniu, H., Pichova, A., & Nystrom, T. (2003). The oncogenic RAS2(val19) mutation locks respiration, independently of PKA, in a mode prone to generate ROS. *Embo J, 22*(13), 3337-3345. doi:10.1093/emboj/cdg314

Hoover, W. G. (1985). Canonical Dynamics - Equilibrium Phase-Space Distributions. *Physical Review A, 31*(3), 1695-1697. doi:DOI 10.1103/PhysRevA.31.1695

Jacobson, M. P., Friesner, R. A., Xiang, Z., & Honig, B. (2002). On the role of the crystal environment in determining protein side-chain conformations. *J Mol Biol, 320*(3), 597-608.

Kong, A. T., Leprevost, F. V., Avtonomov, D. M., Mellacheruvu, D., & Nesvizhskii, A. I. (2017). MSFragger: ultrafast and comprehensive peptide identification in mass spectrometry-based proteomics. *Nat Methods, 14*(5), 513-520. doi:10.1038/nmeth.4256

Li, Z., Vizeacoumar, F. J., Bahr, S., Li, J., Warringer, J., Vizeacoumar, F. S., . . . Boone, C. (2011). Systematic exploration of essential yeast gene function with temperature-sensitive mutants. *Nature biotechnology, 29*(4), 361-367. doi:10.1038/nbt.1832

Longtine, M. S., McKenzie, A., 3rd, Demarini, D. J., Shah, N. G., Wach, A., Brachat, A., . . . Pringle, J. R. (1998). Additional modules for versatile and economical PCR-based gene deletion and modification in Saccharomyces cerevisiae. *Yeast, 14*(10), 953-961. doi:10.1002/(SICI)1097-0061(199807)14:10<953::AID-YEA293>3.0.CO;2-U

Mashhoon, N., Carmel, G., Pflugrath, J. W., & Kuret, J. (2001). Structure of the unliganded cAMP-dependent protein kinase catalytic subunit from Saccharomyces cerevisiae. *Arch Biochem Biophys, 387*(1), 11-19. doi:10.1006/abbi.2000.2241

Mayer, C., Dimopoulos, S., Rudolf, F., & Stelling, J. (2013). Using CellX to Quantify Intracellular Events. *101*(1), 14.22.11-14.22.20. doi:doi:10.1002/0471142727.mb1422s101

Molin, M., Yang, J., Hanzen, S., Toledano, M. B., Labarre, J., & Nystrom, T. (2011). Life span extension and H_2O_2-resistance elicited by caloric restriction require the peroxiredoxin Tsa1 in *Saccharomyces cerevisiae*. *Mol Cell, 43*(5), 823-833. doi:10.1016/j.molcel.2011.07.027

Pan, X., & Heitman, J. (1999). Cyclic AMP-dependent protein kinase regulates pseudohyphal differentiation in Saccharomyces cerevisiae. *Mol Cell Biol, 19*(7), 4874-4887.

Parrinello, M., & Rahman, A. (1981). Polymorphic Transitions in Single-Crystals - a New Molecular-Dynamics Method. *Journal of Applied Physics, 52*(12), 7182-7190. doi:Doi 10.1063/1.328693

Peeters, K., Van Leemputte, F., Fischer, B., Bonini, B. M., Quezada, H., Tsytlonok, M., . . . Thevelein, J. M. (2017). Fructose-1,6-bisphosphate couples glycolytic flux to activation of Ras. *Nat Commun, 8*(1), 922. doi:10.1038/s41467-017-01019-z

Ponder, J. W., & Case, D. A. (2003). Force fields for protein simulations. *Adv Protein Chem, 66*, 27-85.

Rappsilber, J., Mann, M., & Ishihama, Y. (2007). Protocol for micro-purification, enrichment, pre-fractionation and storage of peptides for proteomics using StageTips. *Nat Protoc, 2*(8), 1896-1906. doi:10.1038/nprot.2007.261

Reiter, W., Anrather, D., Dohnal, I., Pichler, P., Veis, J., Grotli, M., . . . Ammerer, G. (2012). Validation of regulated protein phosphorylation events in yeast by quantitative mass spectrometry analysis of purified proteins. *Proteomics, 12*(19-20), 3030-3043. doi:10.1002/pmic.201200185

Salomon-Ferrer, R., Case, D. A., & Walker, R. C. (2013). An overview of the Amber biomolecular simulation package. *Wiley Interdisciplinary Reviews-Computational Molecular Science, 3*(2), 198-210. doi:10.1002/wcms.1121

Sikorski, R. S., & Hieter, P. (1989). A system of shuttle vectors and yeast host strains designed for efficient manipulation of DNA in *Saccharomyces cerevisiae*. *Genetics, 122*(1), 19-27.

Tagwerker, C., Flick, K., Cui, M., Guerrero, C., Dou, Y., Auer, B., . . . Kaiser, P. (2006). A tandem affinity tag for two-step purification under fully denaturing conditions: application in ubiquitin profiling and protein complex identification combined with in vivocross-linking. *Mol Cell Proteomics, 5*(4), 737-748. doi:10.1074/mcp.M500368-MCP200

Tanaka, K., Nakafuku, M., Tamanoi, F., Kaziro, Y., Matsumoto, K., & Toh-e, A. (1990). IRA2, a second gene of Saccharomyces cerevisiae that encodes a protein with a domain homologous to mammalian ras GTPase-activating protein. *Mol Cell Biol, 10*(8), 4303-4313.

Vizcaino, J. A., Csordas, A., del-Toro, N., Dianes, J. A., Griss, J., Lavidas, I., . . . Hermjakob, H. (2016). 2016 update of the PRIDE database and its related tools. *Nucleic Acids Res, 44*(D1), D447-456. doi:10.1093/nar/gkv1145

Voordeckers, K., Kimpe, M., Haesendonckx, S., Louwet, W., Versele, M., & Thevelein, J. M. (2011). Yeast 3-phosphoinositide-dependent protein kinase-1 (PDK1) orthologs Pkh1-3 differentially regulate phosphorylation of protein kinase A (PKA) and the protein kinase B (PKB)/S6K ortholog Sch9. *J Biol Chem, 286*(25), 22017-22027. doi:10.1074/jbc.M110.200071

Zhu, K., Borrelli, K. W., Greenwood, J. R., Day, T., Abel, R., Farid, R. S., & Harder, E. (2014). Docking covalent inhibitors: a parameter free approach to pose prediction and scoring. *J Chem Inf Model, 54*(7), 1932-1940. doi:10.1021/ci500118s